Pb–Zn mineralization in a Miocene regional extensional context: The case of the Sidi Driss and the Douahria ore deposits (Nefza mining district, northern Tunisia)

Sophie Decrée [a,*], Christian Marignac [b,d], Thierry De Putter [c], Etienne Deloule [b], Jean-Paul Liégeois [c], Daniel Demaiffe [a]

[a] *Université Libre de Bruxelles, CP 160/02, Laboratoire de géochimie isotopique-DSTE, 50 av. F. Roosevelt, B-1050 Brussels, Belgium*
[b] *Centre de Recherches Pétrographiques et Géochimiques (CNRS), BP 20-54501 Nancy, France*
[c] *Musée Royal de l'Afrique Centrale, Géologie Isotopique, 13 Leuvensesteenweg, B-3080 Tervuren, Belgium*
[d] *Ecole Nationale Supérieure des Mines de Nancy, Parc de Saurupt, 54042 Nancy, France*

Abstract

The Sidi Driss and Douahria sulfide ore deposits and showings are located in the Nefza mining district, northern Tunisia. The ores are hosted within Upper Miocene (Messinian) basins, within carbonate lenses composed of Fe–Mn-enriched dedolomite partially or totally replaced by early barite and celestite. The ore mainly consists of galena and spherulitic/colloform sphalerite (partially replaced by later Fe-sulfides). It is present as disseminated or banded ores and has been deposited within the host-rock through dissolution/replacement process or through void infilling. The remaining voids are filled by late calcite/barite locally associated with a late oxidation event. *In situ* ion microprobe sulfur isotope analyses show significant variability for sphalerite (from −43.9 to 1.2‰), galena (from −30.3 to −2‰) and marcasite $\delta^{34}S$ (from −35.9 to 25.8‰). These values are interpreted as the result of (i) the mixing of two sulfur end-members in the mineralizing fluids, corresponding to different reduction processes (bacterially-mediated sulfate reduction and thermochemical sulfate reduction, with early celestite and barite and/or contemporaneous Messinian seawater, together with Triassic sulfate, as sulfur sources, and (ii) Rayleigh fractionation process in a closed system.

Several arguments (Fe–Mn enrichment in early diagenetic carbonates, involvement of Messinian seawater as a sulfur source, low temperature of deposition and soft-style sedimentary figures within sulfides) suggest that the Sidi Driss and Douahria Pb–Zn ore deposits are syn-diagenetic. Moreover, the properties of the ore deposits, with Fe–Mn carbonates having a wider distribution than that of the base metal sulfides, and the characteristics of the mineralization, in which diagenetic sulfates are a sulfur source and Cd enrichment in sphalerite, support the classification of the Sidi Driss and Douahria Pb–Zn deposits as SHMS-Sedex type.

Late Miocene extension, comprising rifting dynamics and basalt emplacement, favored a thermally-driven fluid circulation origin for the Sidi Driss and Douahria deposits, enhancing inception of small-scale shallow convection cells. Such sulfide emplacement is significantly different from that of southernmost MVT ore deposits of Tunisia, which are associated with diapirs and are interpreted as the result of a Serravalian–Tortonian gravity-driven fluid circulation event related to late Alpine convergence.
© 2008 Elsevier B.V. All rights reserved.

1. Introduction

In the Nefza region, which belongs to the Nappe Zone of northern Tunisia (Fig. 1), small post-nappe basins host minor Pb–Zn and Fe occurrences and showings (Sidi Driss–Tamra and Douahria). These deposits are spatially and temporally

---

* Corresponding author. Tel.: +32 2 650 22 46; fax: +32 2 650 22 52.
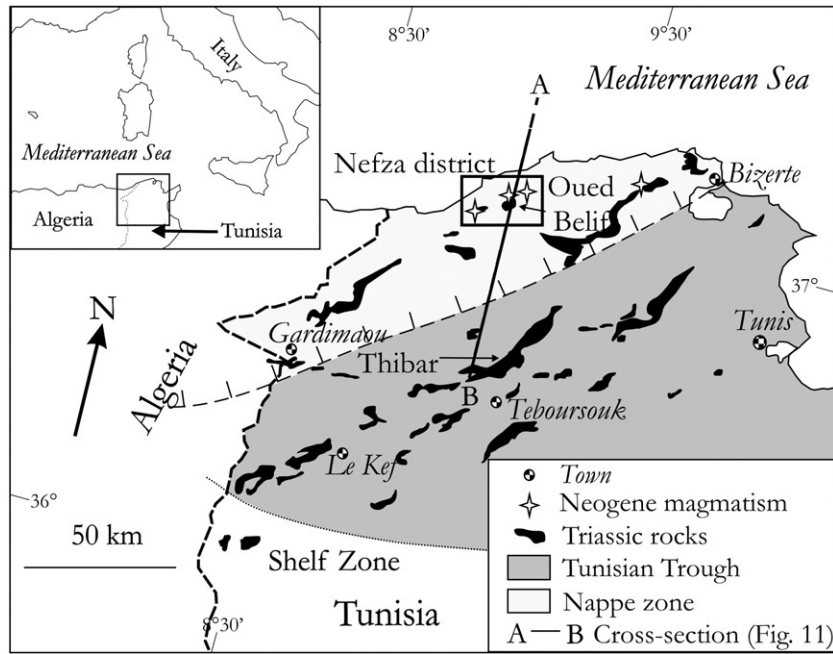*E-mail address:* sdecree@ulb.ac.be (S. Decrée).

Fig. 1. Location map of the studied sites within the main tectono-sedimentary units of northern Tunisia (modified from Rouvier et al., 1985). Section A–B is shown in Fig. 11.

associated with Middle to Late Miocene magmatism of the Nefza area, especially the Haddada rhyolite complex (8.6± 0.3 Ma; Faul and Foland, 1980) and the enigmatic Oued Belif structure (Fig. 2). The latter is an elliptical, 7×3 km-sized ring of ferruginous breccia enclosing a chaotic formation (i.e., variegated and brecciated/highly deformed sedimentary forma-

tions similar to those usually seen in Triassic outcrops; Negra, 1987) and two generations of Middle and Late Miocene subvolcanic rocks (the 12.9 Ma Ragoubet el Alia granodiorite and the 8.3 Ma Ragoubet es Seid rhyodacite; Bellon (1976), Rouvier (1994)). The Oued Belif structure has been variously interpreted as a salt diapir coeval with the magmatism (e.g.,
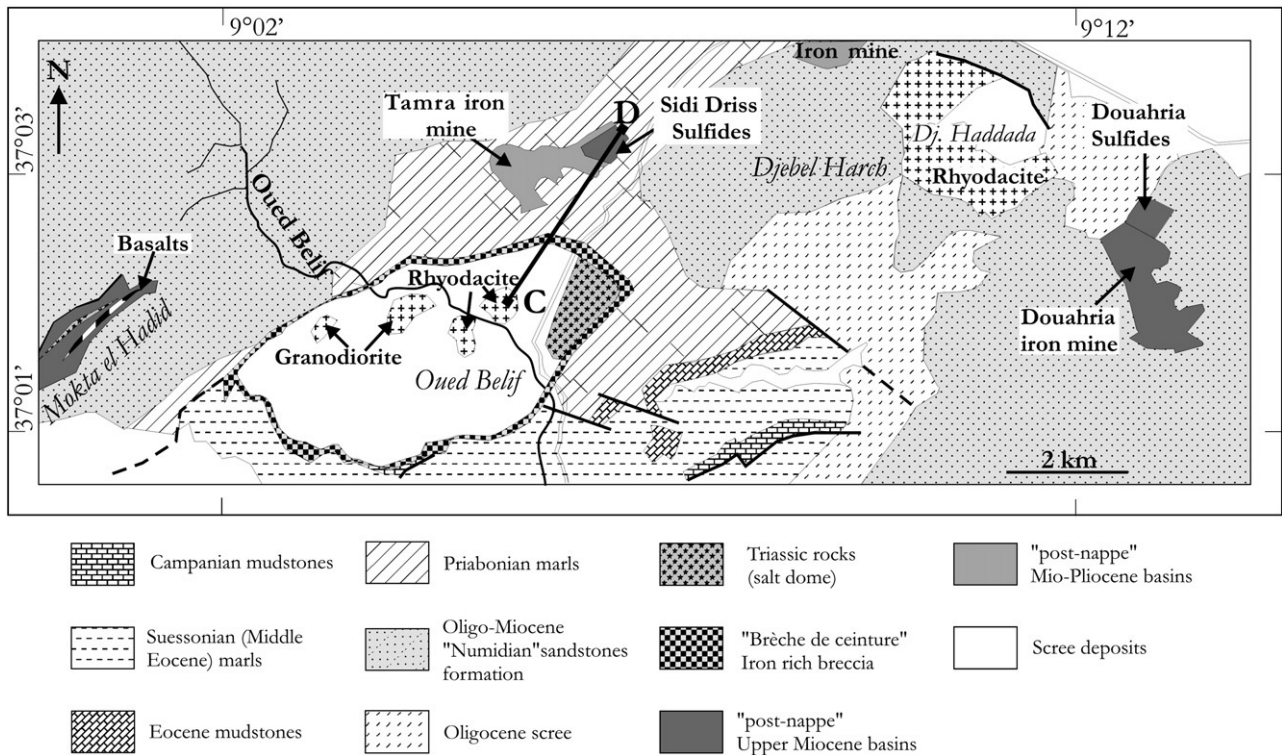

Fig. 2. Geological sketch map of the studied area (modified and redrawn from the geological maps of Gottis and Sainfeld, 1952 and Rouvier, 1987). Line C–D corresponds to the section presented in Fig. 3.

Crampon, 1971) or a caldera (e.g., Talbi et al., 1999); a comprehensive discussion of this enigmatic structure is beyond the scope of this paper. However, the demonstrated presence of diapir-related rocks, including metamorphosed Triassic pelites (Dermech, 1990), does not favor the Miocene-filled caldera hypothesis. On the other hand, since all other Triassic diapirs in northern Tunisia were activated from the Late Cretaceous to the Eocene (e.g., Perthuisot, 1981), it is unlikely that Oued Belif is an exception, and the syn-Miocene diapirism hypothesis is also unlikely. In this contribution, we will present evidence supporting the hypothesis of a thrust-reworked pre-Miocene diapir, as initially suggested by Rouvier (1977) and currently observed in other similar fold-and-thrust belts (e.g., Callot et al., 2005). Recent geophysical work by Jallouli et al. (2003) leads to the recognition of a very shallow concealed magmatic sill (up to 0.7 to 0.9 km thick) under the whole studied area, and which could have been the root of the Haddada and Oued Belif intrusions.

These relationships raise the possibility of a genetic link between the Sidi Driss–Tamra and Douahria ores and Middle to Late Miocene magmatism, as is the case for other polymetallic mineralization in the internal parts of the Maghrebides (e.g., Aïn Barbar and the Edough Massif, northeastern Algeria; Marignac (1988), Aïssa et al. (1998) and Nador Province, Morocco; El Bakkali et al. (1998)). This possibility was also considered by Dermech (1990), whereas Sainfeld (1952) favored a relationship with Triassic evaporites, as in the MVT deposits of the Tunisian Trough Zone (Fig. 1; Rouvier et al., 1985).

The present work, based on new field and laboratory observations and analyses, is a reappraisal of the nature, origin and possible magmatic connection of the Sidi Driss and Douahria sulfide occurrences.

2. Geological setting

In the studied area, the nappe pile is composed of the Kasseb and Ed Diss thrust sheets (Upper Cretaceous to Eocene, alternating limestones and marls), overlain by the Numidian nappe (Rouvier, 1977) (Fig. 2). The latter consists of a thick ($\geq$1000 m) series of silicoclastic flyschs (the so-called Numidian flysch, made up of sandstones and argilites), which is of Oligocene to Burdigalian age. The nappe pile is crosscut by felsic plugs and mafic dikes and sills (Mauduit, 1978) of the

Late Miocene and Pliocene Nefza magmatic province (Jallouli et al., 2003 and references therein); basaltic flows are also known. The Oued Belif structure also crosscuts the nappe pile since Numidian blocks have been reported within the ferruginous ring breccia (e.g., Negra, 1987).

The small Sidi Driss–Tamra and Douahria basins unconformably overlie the eroded nappe pile (Figs. 2 and 3). Detailed lithological sequences are given in Fig. 4. According to Stefanov and Ouchev (1972) and Dermech (1990), the Sidi Driss basin is presently a syncline, with longitudinal NE-SW faults that are deemed to have been active during sedimentation. As shown in Figs. 3 and 4, marls are the dominant rock type, with several intercalations of conglomerates, supratidal limestones and evaporites. A first volcanoclastic horizon in the lower part of the basin is characterized by numerous rounded pebbles of calcitised rhyodacite material (Dermech, 1990), associated with clasts from both the nappe substratum (Numidian sandstones) and the saliferous complex of Oued Belif (metamorphosed Triassic pelites). A thin horizon is, however, interpreted as a tuffaceous horizon (iron-stained lapilli; Dermech, 1990). According to thickness variations, the volcanic material was emitted from the southwest, i.e., probably from the Ragoubet es Seid rhyodacite in the Oued Belif structure (Fig. 3), while marine inflows brought sediments from the northern edge of the basin. Higher in the pile, a second conglomeratic horizon is found, with limestone clasts from the Ed Diss unit ("mineralized layer 2" of Dermech, 1990). Towards the top of the pile, a supratidal limestone horizon of variable thickness consists of an intercalated stromatolitic and micritic facies ("mineralized layer 1" of Dermech, 1990), which will be described in more detail below. Anhydrite ghosts are numerous in the algal mats and testify to an evaporitic (sabkha or salina) environment. Higher in the series, conglomeratic lenses and several discontinuous limestone layers are intercalated within the marls in the northeastern part of the basin (Fig. 3). Two thin, metre-scale evaporite horizons and more or less continuous lenses of celestite are also present within the marls, below and above conglomeratic layer 2. In the upper part of the basin, the presence of lignite, lenticular horizons and cross-stratifications led Sainfeld (1952) to propose a Messinian age. The formations of the Sidi Driss basin are unconformably overlain by the ferruginous formations of the Mio-Pliocene Tamra basin (Decrée et al., in press).
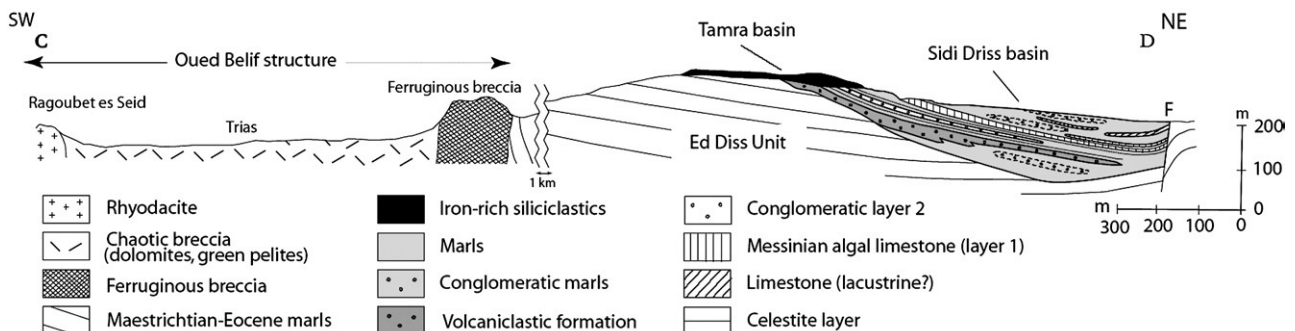

Fig. 3. Schematic cross-section of the Sidi Driss–Tamra zone along the profile C–D (see Fig. 2). Infill of the Sidi Driss basin is schematized after Stefanov and Ouchev (1972) and Dermech (1990).
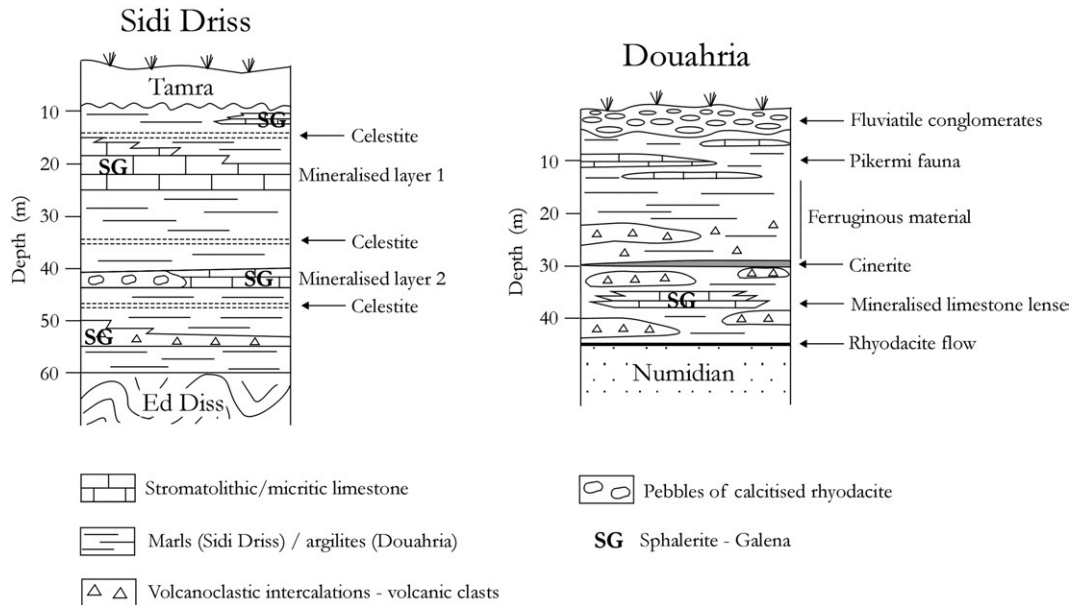
Fig. 4. Comparative lithologic logs of the basin filling sequences of Sidi Driss and Douahria, where the mineralized bodies are indicated by SG (sphalerite–galena). Modified after Dermech (1990), Negra (1987) and Vassileff and Popov (1979).

According to Vassileff and Popov (1979) and Negra (1987), the Douahria basin is a small graben that was filled first by a thick unit of marls with numerous volcanoclastic intercalations, then by argillites, with thin lenticular limestone intercalations towards the top (Fig. 4). The argillites contain remnants of a terrestrial mammal fauna dated from the latest Messinian (Pikermi fauna; Roman and Solignac, 1934; Jaeger, 1977). In the volcanoclastic intercalations, the volcanic clasts are more or less altered rhyodacites, likely derived from the nearby Haddada rhyodacites. We have observed rhyodacite flows, a few tens of cm thick, which flooded weathered Numidian argilites close to one of the border faults. The upper part of the volcanoclastic unit contains silicified cinerite and tuff levels (Vassileff and Popov, 1979; Negra, 1987) and widespread ferruginous impregnations. It is thus known as the "ferruginous formation" (Negra, 1987). Intercalated towards the basis of this "ferruginous formation", there is a thin lenticular shallow marine limestone horizon (micritic and anhydrite-bearing stromatolitic limestone, according to our observations) which hosts the Douahria Pb–Zn ore occurrence. A sequence of fluviatile silicoclastic deposits, ranging from conglomerates to fine-grained sandstones, rests unconformably on these sediments, and is the last recorded formation in the Douahria basin. It may correlate with the continental sequence above the deposits in the Sidi Driss basin.

Despite these differences, the two basins display some similarities. (1) In both, sedimentation was mainly Messinian in age, possibly encompassing the late Tortonian. Indeed, the Douahria deposit series comprises volcanoclastic formations derived from subaerial protrusions and flows of the Tortonian rhyodacite, and indications of coeval volcanic activity are present (cinerites, tuffaceous beds). The Douahria basin was, however, more proximal to the volcanic source. (2) In the two basins, the depositional environment was generally shallow,

with alternating continental deposits and shallow marine inflowing sediments; both series end with a fully continental, fluviatile, environment. (3) In the two basins, Zn–Pb sulfide mineralization is found in horizons of shallow marine limestones bearing the same sedimentological character (interbedded micritic and anhydrite-bearing stromatolitic limestones; our observations). These similarities led Rouvier (1994) to propose that the present-day basins of Sidi Driss–Tamra and Douahria are actually isolated remnants of a larger, pre-existing basin. These arguments are, however, too weak to categorically discard the alternative interpretation that each basin represents an independent depocentre.

3. Previous work on the Zn–Pb–Fe mineralization

Although exploited for more than a century, the Sidi Driss Zn–Pb sulfide deposit was closed 30 years ago and is now exhausted. A few studies were devoted to the geology and origin of the deposit. Sainfeld (1952) and Gottis and Sainfeld (1952) were the first to give a description and to propose a genetic model. In the 1970's, the Tunisian National Mine Office (ONM) performed a series of exploratory drillings (Stefanov and Ouchev, 1972; Negra, 1987; Dermech, 1990). Two additional cores were drilled in 1981 (Dermech, 1990). Finally, Negra (1987) and Dermech (1990) summarized the existing data and worked on the Tamra, Douahria and Sidi Driss mines and on the Oued Belif structure and related ferruginous breccias. In the Douahria basin, the Zn–Pb sulfide exposures, mined a long time ago, were merely mentioned by Negra (1987). Several authors (Berthon, 1922; Vassileff and Popov, 1979; Negra, 1987) worked on the ferruginous mineralization. The Tamra ferruginous formation is described by Decrée et al. (in press), concluding that the Tamra iron ore resulted from the combination of a pedogenetic pre-concentration, followed by a

Table 1
Representative microprobe analyses (wt.%) and atomic proportions (at.%) for carbonates from Sidi Driss and Douahria

| | Sidi Driss | | | | | | | | | | | | Douahria | | | | |
| | Carbonate host-rocks | | | | | | Calcite infillings (C.I.) | | | | | | Carbonate host-rocks | | | C.I. | |
	SD2b-C2	SD2b-C3	SD5b-C2	SD5b-C3	SD2b-C6	SD2b-C5	SD5b-C4	SD2a-C1	SD2a-C4	SD2a-C5	SD5-C3	SD5-C1	DSU7-C8	DSU7-C11	DSU2-C5	DSU7-C13	d.l. (ppm)
wt.%																	
Ca	40.50	40.09	36.51	40.34	19.04	4.04	39.25	38.39	40.02	41.60	40.36	38.51	40.03	40.88	4.55	40.18	590
Sr	0.97	0.40	<d.l.	0.37	0.58	0.20	0.23	0.61	0.21	0.75	0.19	0.40	0.05	0.63	0.16	0.17	1330
Mg	<d.l.	<d.l.	<d.l.	0.06	7.66	0.39	<d.l.	<d.l.	0.07	0.09	<d.l.	0.03	0.13	<d.l.	0.88	0.07	530
Fe	<d.l.	1.61	4.97	1.27	9.64	31.91	1.05	1.02	1.54	<d.l.	1.66	3.34	1.97	<d.l.	36.22	0.81	3470
Mn	<d.l.	1.41	1.84	1.40	2.28	6.77	2.35	1.85	0.80	0.55	0.77	1.62	0.81	<d.l.	1.22	<d.l.	3450
S	0.20	0.06	0.10	0.03	<d.l.	<d.l.	<d.l.	<d.l.	0.08	0.07	<d.l.	0.07	<d.l.	0.25	0.07	<d.l.	260
Sum	41.67	43.57	43.42	43.46	39.20	43.31	42.89	41.87	42.71	43.05	42.98	43.96	42.99	41.75	43.09	41.23	
at.%																	
Ca	0.983	0.941	0.879	0.947	0.470	0.125	0.938	0.941	0.952	0.977	0.955	0.908	0.947	0.986	0.138	0.980	
Sr	0.011	0.004	0.000	0.004	0.006	0.003	0.003	0.007	0.002	0.008	0.002	0.004	0.001	0.007	0.002	0.002	
Mg	0.000	0.001	0.001	0.002	0.312	0.020	0.001	0.001	0.003	0.003	0.001	0.001	0.005	0.000	0.044	0.003	
Fe	0.000	0.027	0.086	0.021	0.171	0.702	0.018	0.018	0.026	0.000	0.028	0.057	0.033	0.000	0.787	0.015	
Mn	0.000	0.024	0.032	0.024	0.041	0.151	0.041	0.033	0.014	0.009	0.013	0.028	0.014	0.000	0.027	0.000	
S	0.006	0.002	0.003	0.001	0.000	0.000	0.000	0.000	0.002	0.002	0.000	0.002	0.000	0.007	0.003	0.000	

d.l.=Detection limit and <d.l. corresponds to values below the detection limit.

hydrothermal iron deposition in a basin superimposed onto the Sidi Driss basin.

At Sidi Driss, the Zn–Pb–(Ba) mineralization occurs at several horizons in the sedimentary pile within the volcanoclastic formations, and in two carbonate horizons (layers 2 and 1; Fig. 4). The volcanoclastic intercalation and the mineralized layer 2 are currently not accessible; available information comes only from the work of Dermech (1990). According to that author, two types of mineralization can be sporadically found within the volcanoclastic layers, after the diagenetic crystallization of Fe-rich carbonates and pyrite: (i) barite encrusting the Fe-carbonates in vugs and (ii) (rare) sphalerite–calcite veinlets. In the mineralized layer 2, a diagenetic crystallization of Fe-rich calcite also occurred in the conglomerate matrix, followed by veinlets successively filled with sphalerite, galena and calcite in the southwest of the mine area, and by galena and barite replacements of the matrix, with subordinated veinlets of the same minerals in the northeast; barite is later than galena.

4. Material and methods

Although mineralized outcrops and workings in Sidi Driss are nowadays poorly exposed and the Sidi Driss galleries are collapsed, *in situ* sampling was still possible. This allowed a rough reconstruction of the deposit. In Douahria, the mine constitutes the only source of information, the ONM drill cores being no more available. Forty rock samples were collected in 2004 and 2005. The mineralogy and textures of the rocks were determined using reflected light microscopy and were further investigated by scanning electron microscopy. Chemical data (Tables 1 to 4) were obtained using a CAMECA SX100 electron microprobe. Both SEM and microprobe are located at the "Service Commun de Microanalyse" facility of the Henri Poincaré-Nancy1 University, France.

Sulfur isotopic compositions ($\delta^{34}S$) were analyzed using the CRPG-CNRS Cameca IMS1270 ion microprobe. A $^{133}Cs^+$ primary beam with 20 kV incident energy (10 kV primary, 10 kV secondary) was used in defocused aperture illumination mode, producing a ca. 20 µm spot, together with the normal incidence electron gun in self-compensation mode (i.e., with incident energy ca. 0 kV) in order to avoid any charge build up during the analysis. To achieve a good reproducibility, each analysis was preceded by an automated centering of the sample spot image in the field aperture (Schuhmacher et al., 2004). Negative secondary ions with an energy spread of ca. 40 eV were analyzed at mass resolution (M/DM) of 3000, sufficient to

Table 2
Representative microprobe analyses (elements in wt.%) and atomic proportions (at.%) of barite and celestite from Sidi Driss and Douahria

| | Sidi Driss | | | Douahria | | | | |
| | Barite host-rocks | | Celestite host-rock | Celestite host-rock | Barite replacement/infillings | | | |
	SD5-C2	SD2-C6	SD2b-C1	DSU2-C3	DSU7-C20	DSU7-C18	DSU7-C17	d.l. (ppm)
wt.%								
Ba	61.44	62.25	<d.l.	<d.l.	65.24	61.93	65.08	3520
Sr	2.53	2.78	48.08	49.39	0.48	4.41	0.52	1820
Ca	0.05	0.07	0.10	0.05	0.08	0.36	<d.l.	460
S	13.43	13.46	17.22	17.28	13.71	13.58	13.24	460
Sum	77.45	78.55	65.40	66.71	79.51	80.28	78.84	
at.%								
Ba	0.999	1.001	0.000	0.001	1.045	0.967	1.063	
Sr	0.064	0.070	1.010	1.022	0.012	0.109	0.014	
Ca	0.002	0.004	0.005	0.002	0.004	0.019	0.000	
S	0.934	0.926	0.985	0.975	0.939	0.905	0.923	

d.l.=Detection limit and <d.l. corresponds to values below the detection limit.

Table 3

Representative microprobe analyses (elements in wt.%) and atomic proportions (at.%) of sphalerite from Sidi Driss and Douahria

	Sidi Driss										Douahria				
	Carbonate-hosted sphalerite spherules					Carbonate-hosted sphalerite colloform band		Sulfate-hosted sphalerite spherules			Carbonate-hosted sphalerite spherules				
	SD2a-S3	SD5b-S1	SD5b-S7	SD2a-S10	SD2a-S11	SD2a-S16	SD2a-S8	SD5-S3	SD5-S6	SD2-S5	DSU7-S5	DSU7-S8	DSU6-S3	DSU6-S5	d.l. (ppm)
wt.%															
Zn	66.34	65.68	65.96	66.26	65.21	66.11	66.24	63.78	64.87	64.74	67.12	66.68	66.43	66.04	7410
Fe	<d.l.	0.94	1.03	<d.l.	<d.l.	<d.l.	<d.l.	1.67	0.55	<d.l.	<d.l.	<d.l.	<d.l.	<d.l.	3520
Cd	0.38	0.51	0.13	0.10	0.95	0.13	0.74	0.65	0.22	0.79	0.10	0.11	0.45	0.38	910
S	33.27	32.87	32.88	33.64	33.85	33.76	33.02	33.90	34.36	34.47	32.78	33.22	33.12	33.58	1310
Sum	100.00	100.00	100.00	100.00	100.00	100.00	100.00	100.00	100.00	100.00	100.00	100.00	100.00	100.00	
at.%															
Zn	0.988	0.980	0.983	0.983	0.968	0.980	0.989	0.944	0.956	0.956	1.002	0.992	0.990	0.981	
Fe	0.000	0.016	0.018	0.000	0.000	0.000	0.000	0.029	0.010	0.000	0.000	0.000	0.000	0.000	
Cd	0.003	0.004	0.001	0.001	0.008	0.001	0.006	0.006	0.002	0.007	0.001	0.001	0.004	0.003	
S	1.009	0.999	0.998	1.016	1.024	1.019	1.005	1.022	1.032	1.037	0.997	1.007	1.006	1.016	

Due to significant As contamination in the course of the metallization process, the As content has been subtracted, in order to allow for a correct computation of the structural formula of the analyzed sulfides (i.e. the sum of the other elements has been rounded to 100%).
<d.l. corresponds to values below the detection limit.

resolve ^{34}S from ^{33}SH. ^{32}S and ^{34}S were measured simultaneously on two Faraday cups. Each analysis consisted of 180 s of pre-sputtering, followed by 180 s of beam integration. The measured ^{34}S/^{32}S ratio is corrected for instrumental and matrix related mass bias using reference sulfide and sulfate (Car111 for pyrite, ISH9 for galena and Anhydrite Cuney for sulfates). In a first step, sulfur isotopes punctual analyses were performed on eighteen separate minerals (6 sulfates, 7 galena and 7 Fe-sulfides), with at least two analyses/sample. Due to the small size of the sphalerite spherules and aggregates (see below), they could not be separated for δ^{34}S measurement. Therefore, a series of preliminary *in situ* point analyses were performed on sphalerite spherules aggregates (Filoche and Flinois, 2007).

5. Description of the ores

5.1. Ca-evaporitic/dolomite host-rocks and early diagenetic replacements

At Sidi Driss, the studied carbonate-hosted sulfide mineralization (Fig. 5) corresponds to the first (no 1) mineralized horizon of Dermech (1990). Host carbonates are: (i) highly recrystallized algal boundstones that are made up from dedolomicrosparite, with vuggy laminated horizons of micritic peloids and rare recrystallized bioclasts. They contain evaporite remnants (some calcite pseudomorphs after gypsum biconvex lenses are still visible); and (ii) roughly laminated matrix-supported conglomerates containing clasts of quartz and glauconite (74.87 wt.% SiO_2, 11.53 wt.% Al_2O_3, 0.86 wt.% FeO, 0.81 wt.% MgO, 1.69 wt.% CaO, 0.40 wt.% Na_2O and 1.13 wt.% K_2O) and mm to cm-size, rounded celestite (inducing loadcast structures) in a matrix of fine-grained carbonates. Microprobe analyses reveal the presence of two different calcites, with distinct Fe–Mn contents (0 to 1.61 wt.% Fe and 0

to 1.41 wt.% Mn for boundstone (analyses SD2b-C2 and C3; Table 1) and 1.27 to 4.97 wt.% Fe and 1.40 to 1.84 wt.% Mn for conglomerate matrix (analyses SD5b-C2 and C3; Table 1), coexist in both rock types. Within the conglomeratic facies, another carbonate phase is locally observed, either within the matrix or in the silicate clasts (quartz and glauconite, details in Fig. 5F). This carbonate has a rhombohedral habit (up to 15 μm

Table 4

Representative microprobe analyses (elements in wt.%) and atomic proportions (at.%) of Fe-sulfides from Sidi Driss and Douahria

	Sidi Driss					Douahria		
	Marcasite replacing sulfides (M.R.S.)		Marcasite/pyrite infillings (M.I.)			M.R.S.	M.I.	
	SD5b-S4	SD5-S11	SD5b-S11	SD2a-S17	SD5-S7	DSU7-S4	DSU7-S1	d.l. (ppm)
wt.%								
Fe	44.54	45.30	46.61	46.50	45.98	45.03	47.36	4330
Zn	<d.l.	<d.l.	<d.l.	<d.l.	<d.l.	0.90	<d.l.	6680
Pb	0.84	1.77	<d.l.	<d.l.	<d.l.	1.54	<d.l.	5890
As	4.55	0.55	<d.l.	<d.l.	<d.l.	0.64	<d.l.	1520
S	50.06	52.38	53.39	53.50	54.02	51.89	52.64	1480
Total	100.00	100.00	100.00	100.00	100.00	100.00	100.00	
at.%								
Fe	0.995	0.990	1.000	1.000	1.000	0.974	1.000	
Zn	0.000	0.000	0.000	0.000	0.000	0.017	0.000	
Pb	0.005	0.010	0.000	0.000	0.000	0.009	0.000	
As	0.076	0.009	0.000	0.000	0.000	0.010	0.000	
S	1.944	1.989	1.991	2.000	2.042	1.952	1.932	

As in Table 3, the sum of measured elements has been rounded to 100%, allowing however, in this case for the presence of As in the structural formula of these sulfides.
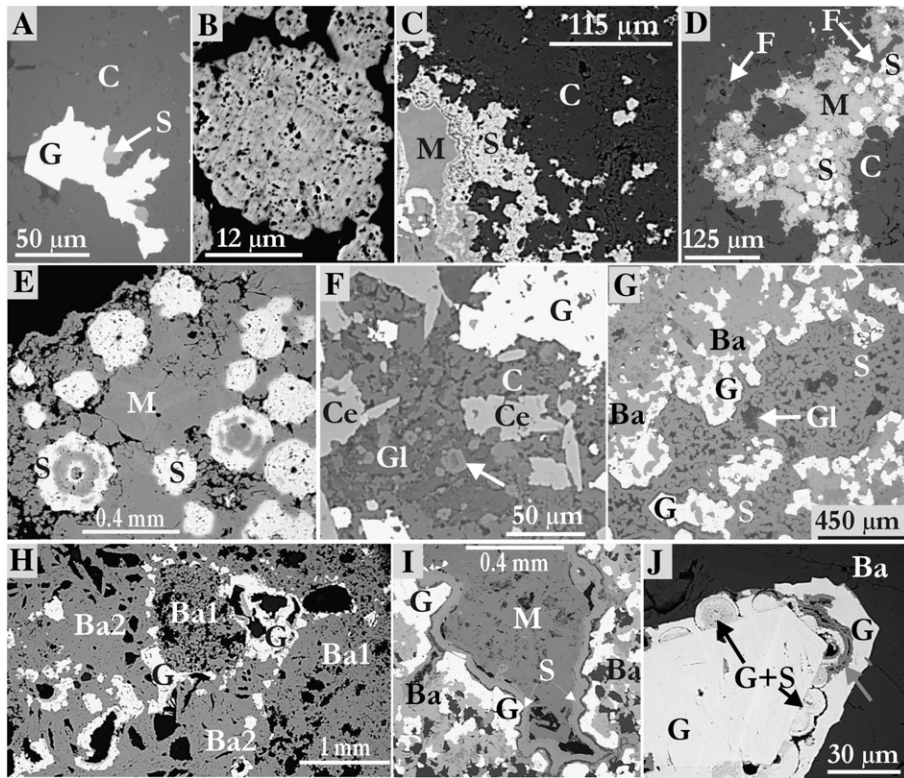d.l. = Detection limit and <d.l. corresponds to values below the detection limit.

Fig. 5. Backscattered electrons images of disseminated/massive ores within carbonate and sulfate host-rocks from Sidi Driss. "Ba" and "Ba1" indicate barite host-rocks and "Ba2" correspond to later barite infillings. "C", "Ce", "F", "G", "Gl", "M" and "S" indicate carbonate host-rock, celestite, fluorite, galena, glauconite+quartz, marcasite and sphalerite, respectively. (A). Anhedral galena and sphalerite spherule disseminated within carbonate host-rock (sample SD5b). (B). Detail of a typical sphalerite spherule within carbonate (sample SD5b). (C). Disseminated sphalerite spherules within the carbonate host-rock (right part of figure) that coalesce to form wider patches in the vicinity of voids (left part of figure). The remaining void was later infilled by marcasite (sample SD5b). (D). Massive replacement of the carbonate matrix by sphalerite spherules and later marcasite. Fluorite is present in association with sphalerite or as isolated crystals replacing the carbonate (sample SD5b). (E). Sphalerite spherules surrounded by coalescing marcasite and partially replaced by the same mineral (sample SD5b). (F). Complex host-rock for galena ore, constituted by carbonate, partly replaced by celestite, glauconite patches and zoned ankerite rhombohedra (white arrow) (sample SD2a). (G). Barite host-rock replaced by galena in the vicinity of voids. Galena is lined with colloform sphalerite; the remaining void is filled with sphalerite spherules before a final glauconite+quartz infilling (sample SD5). (H). Fine-grained residual barite matrix (Ba1) surrounded by replacing galena before the emplacement of large barite laths (Ba2) (sample SD5). (I). Galena replacing barite matrix on the edge of voids, lined with a sphalerite colloform band; the remaining void is filled with marcasite (Ba–G–S–M, sample SD5). (J). Galena crystal within barite host-rock, surrounded by sphalerite spherules (partly replaced by later galena), in turn entrapped in a later galena crystal (sample SD2).

in length) with a distinct zoning: an ankerite core (7.66 wt.% Mg and 9.64 wt.% Fe, analysis SD2b-C6; Table 1) is rimmed by Mn-siderite (31.91 wt.% Fe and 6.77 wt.% Mn, analysis SD2b-C5; Table 1). Rounded residual pre-existing pockets of ankerite rhombohedra (determined by microprobe analysis) were also found within other samples, which are mainly made up from barite. Though rare, this carbonate facies could represent remains of the initial sediment, most probably dolomite.

At Douahria, the host carbonates are highly recrystallized limestones, consisting of euhedral to subhedral Fe–Mn calcite (up to 120 μm). SEM examination reveals several growth zones (Fig. 6A), with alternation of lighter and darker bands reflecting small variations in Mn and/or Fe content (from nearly pure calcite to carbonate having 1.97 wt.% Fe and 0.81 wt.% Mn, analysis DSU7-C8 and C11, Table 1). There is some evidence of pre-existing textures: (i) rare radiating and/or felted laths ("patchwork") of a highly birefringent calcite, interpreted as pseudomorphs after anhydrite, and (ii) large subhedral to euhedral (a few 100 μm in length) rhomb-shaped dedolomite crystals. Additionally, small euhedral (rhombohedral?) Mn-

bearing siderite crystals (20 μm in size, 36.22 wt.% Fe and 1.22 wt.% Mn, analysis DSU2-C5, Table 1) are included within the later celestite crystals (detail in Fig. 6G).

In both basins, the presence of dedolomite and Mg-bearing carbonate rhombohedra demonstrate that dolomite was the initial sediment. Conversion of dolomite into dedolomite took place during early diagenesis. Concurrent with Mg loss, there was a Fe–Mn gain that led to formation of Fe–Mn carbonates, or of pure calcite (in the absence of Fe–Mn gain). These carbonates then hosted a later sulfate/sulfide mineralization. Dolomite conversion into calcite (so-called dedolomitization) is a well-known process that usually takes place when dolomite comes into contact with meteoric fluids (Sanz-Rubio et al., 2001). In the study area, this contact was highly favored by the very shallow depositional environment of the basins. The observed Fe–Mn enrichments, however, suggest a more complex interaction, in which meteoric fluids could be mixed with upward driven Fe–Mn-enriched hydrothermal fluids.

These early diagenetic carbonates were in turn partially or totally replaced by sulfates, prior to the sulfide mineralization.
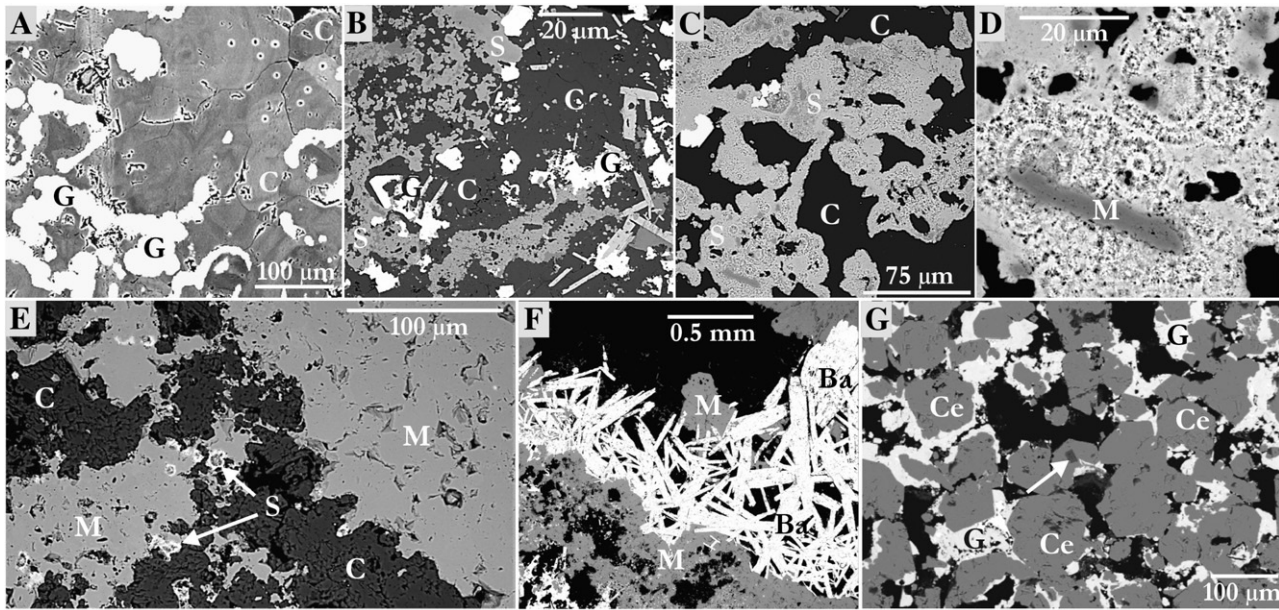
Fig. 6. Backscattered electron images of ores from Douahria (sample DSU7, except figure G from sample DSU2). "Ba", "C", "Ce", "G", "M" and "S" stand for barite, carbonate host-rock, celestite host-rock, galena, marcasite and sphalerite, respectively. (A). Recrystallized carbonate host-rock showing zoned crystals (variations in Mn and/or Fe content), predating galena mineralization. (B). Disseminated sphalerite spherules, galena crystals and barite laths (right part of figure) within carbonate. (C). Coalesced sphalerite spherules forming amoeboid aggregates within the carbonates. (D). Detail of a sphalerite spherule aggregate within the carbonates; the aggregate is partially replaced by marcasite. (E). A marcasite "pseudo-vein" replacing carbonates (right part of figure) and sphalerite spherules (central part of figure). (F). Infilling of the marcasite "pseudo-vein" by barite laths. (G). Galena (sometimes oxidized) surrounding and partially replacing the celestite matrix. White arrow indicates a siderite crystal inside a celestite grain.

The sulfates still retain some typical textures of the initial carbonates (e.g., rhomb-shaped barite and celestite after initial dolomite, and anhydrite-felted laths pseudomorphs). At Sidi Driss, barite is the most abundant sulfate. It is Sr-rich (~2.6 wt. % Sr, SD5-C2 and SD2-C6 analyses, Table 2) and occurs as (i) massive stratabound ore, made up from equigranular aggregates (10 to 50 μm, Fig. 5G) or (ii) dense network of tiny laths (up to 0.15 mm long, Ba1 in Fig. 5H) forming rounded patches (up to 5 mm) or bands (up to 3 mm in size). The dissolution cavities are sometimes filled by a second (post-sulfide) barite generation (Ba2), which occurs as a network of larger (than Ba1) laths surrounding these patches (Fig. 5H). Celestite is less abundant in Sidi Driss, and is present within carbonate rocks as either disseminated euhedral crystals (25 to 60 μm in length, analysis SD2b-C1, Table 2) or as wider patches of aggregated crystals (Fig. 5F). By contrast, at Douahria, celestite is the most abundant sulfate, and barite is apparently a late phase (therefore likely coeval with Ba2 at Sidi Driss). Celestite forms massive layers consisting in aggregates of equigranular euhedral crystals (100 μm in size, or more, Fig. 6G) that replace carbonates (analysis DSU2-C3 in Table 2).

In conclusion, there is evidence – in both the Sidi Driss and Douahria basins – for an early two-stage diagenetic evolution that largely overprinted the original sediment, made up of associated Ca-sulfates and dolomite. In a first step, dolomite was converted into Fe–Mn-bearing dedolomite, that was in turn replaced by a new generation of Ba/Sr-sulfates. Although carbonate replacement is obvious, late sulfates may also have evolved from early Ca-sulfates. In particular, massive barite or celestite layers may be derived from earlier gypsum layers.

Secondary gypsum lenses were described in the marly layers of Sidi Driss by Dermech (1990).

5.2. Zn–Pb–Fe-sulfides

Zn–Pb–Fe-sulfides are hosted either within early diagenetic carbonates, in the secondary sulfates, or in both. They are always stratabound. At Sidi Driss, carbonate-hosted mineralization is dominant with subordinated, although significant, barite-hosted sulfides; at Douahria, celestite-hosted mineralization is by far the most important.

5.2.1. Sidi Driss carbonate-hosted mineralization

The carbonate-hosted sulfides occur either as disseminated patches or as layers.

(i) The typical disseminated stratabound sulfides occur within diagenetic carbonates and consist of Fe-poor, Cd-enriched sphalerite spherules (10 to 30 μm in diameter, 0.38 to 0.51 wt.% Cd and up to 0.94 wt.% Fe, analyses SD2a-S3 and SD5b-S1, Table 3) and of anhedral to subhedral galena crystals (7 to 25 μm, rarely 40 μm) replacing the carbonates (Fig. 5A, B). Fluorite is sometimes associated with these sulfides as small anhedral to subhedral crystals (up to 40 μm; Fig. 5D). More massive dissolution/replacement occurs in the vicinity of some large voids: disseminated sulfides coalesce to form wide patches of aggregated sphalerite spherules (up to 30 μm in diameter) associated with fluorite grains (up to 20 μm in width; Fig. 5D), which are surrounded by coalescing,

radiated As-bearing marcasite crystals (analysis SD5b-S4, Table 4; Fig. 5D). The Fe-sulfides partially replace the sphalerite in these aggregates (Fig. 5E). The latter is less enriched in Cd (0.13 wt.% Cd, analysis SD5b-S7, Table 3) than that occurring within the matrix (analysis SD2a-S3 and SD5b-S1). The voids are rimmed by galena crystals (up to 0.5 mm, partially replaced by Fe-sulfide) surrounded by a thin colloform sphalerite band (up to 50 μm in width). Two successive generations of marcasite

and/or calcite were emplaced later, filling the inner part of the voids. Marcasite is present as colloform bands (20 to 50 μm in width) or as massive fillings with virtually no As in individual crystals (analysis SD5b-S11, Table 4; Fig. 5C). Calcite displays a typical sparitic facies, with Mn contents of 3.35 wt.% (analysis SD5b-C4, Table 1). An uncommon alternative to this typical mineralization consists of partial replacement of carbonates and minor celestite by disseminated crystals and irregular patches of
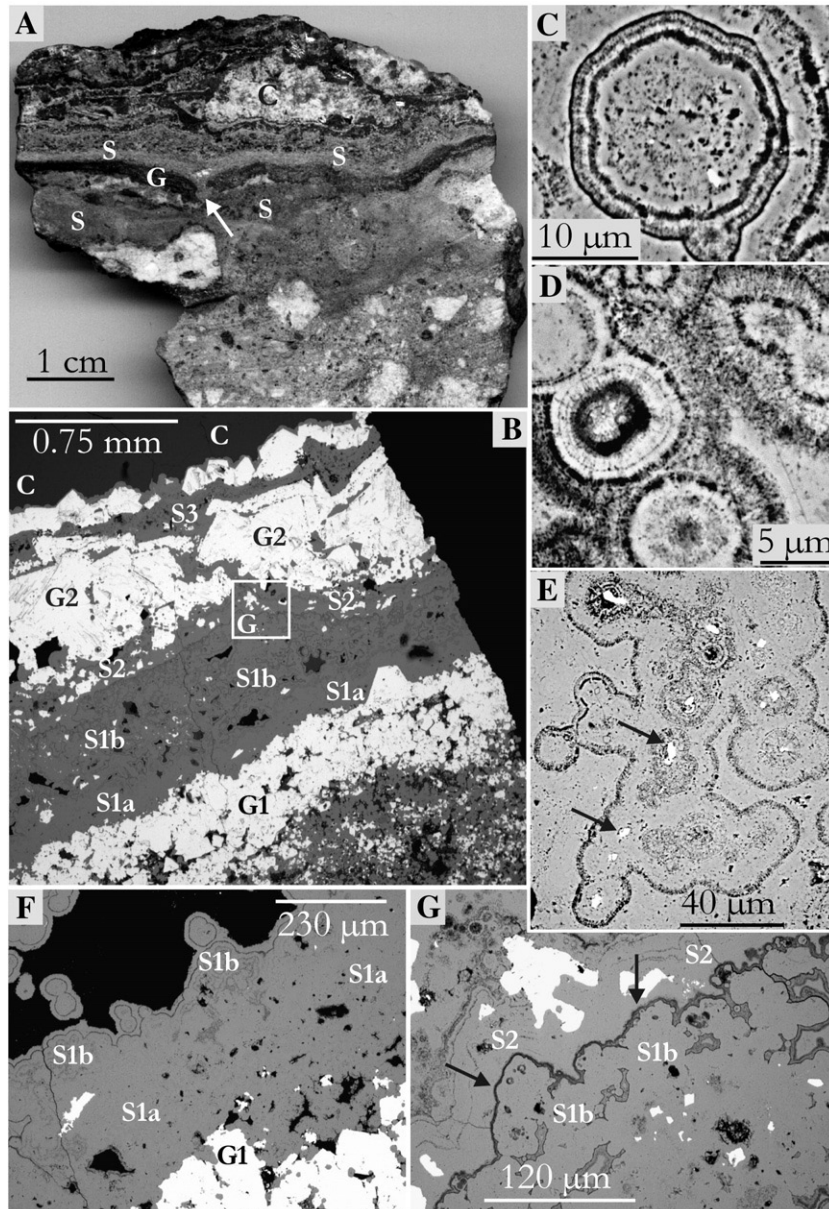
Fig. 7. Photomacrograph (A) and backscattered electron images (B to G) of the banded ores from Sidi Driss (sample SD2a). (A). Alternating galena (G) and sphalerite (S) layers showing early soft deformation (loadcast indicated by white arrow). These overlie disseminated stratabound ore occurring in a complex carbonate host-rock; above the G and S layers, remaining voids are filled with calcite (C). (B). Low-magnification image of the banded ores, where S1a and S2 are colloform sphalerite layers, S1b and S3 correspond to spherulitic sphalerite layers, and G1 and G2 indicate euhedral galena layers; remaining voids are filled with calcite (C). (C). Sphalerite spherules characteristic of the S1b layer; darker bands are due to mixing of sphalerite with a silicate phase, probably kaolinite. (D). Sphalerite spherules characteristic of the S1b layer (darker bands result from the mixing with a silicate phase, probably kaolinite). (E). Same as D; black arrows indicate subhedral galena crystals replacing sphalerite in the porous central part of the spherules. (F). Progressive transition between colloform (S1a) and spherulitic (S1b) sphalerite facies. (G). Sharp transition (indicated by black arrows) between spherulitic (S1b) and colloform (S2) sphalerite facies; the darker color of this transition is due to some mixing of sphalerite with a silicate phase, probably kaolinite.

galena (15 to 30 μm, exceptionally 120 μm; Fig. 5F). Although the estimation is deduced from the limited data at hand, sulfide abundances are in the apparent order: sphalerite > galena > marcasite.

(ii) Sample SD2a was chosen as representative for a detailed description of the banded ores. In this sample, the banded ore overlies a disseminated stratabound ore. It consists of rhythmic alternation of thin sphalerite and galena layers (0.4 to 3 mm), displaying evidence of early soft deformation, e.g., loadcast figures within a galena layer (Fig. 7A). There are two types of sphalerite layers. The first consists of spherules (10 to 30 μm in diameter) or spherule aggregates (Fig. 7C, E) of Fe-poor sphalerite with variable Cd contents (0.10 wt.% Cd for S1b and 0.95 wt.% Cd for S3, analyses SD2a-S10 and SD2a-S11, Table 3). The spherules exhibit both concentric and radial growth structures (Fig. 7C, D). Some dark μm-thick concentric layers contain an undetermined Al-rich silicate (likely kaolinite) or carbonate. A replaced rhombic mineral (dolomite ghost?) is occasionally found in the centre of the spherule. The second type of layer consists of colloform bands (up to 2.5 mm in width; "S1a" in Fig. 7B and F, and "S2" in Fig. 7B and G) of a Fe-poor sphalerite that also displays a wide range in Cd contents from one band to the other (from 0.13 wt.% for "S4" to 0.74 wt.% Cd for "S1a", analyses SD2a-S16 and SD2a-S8, Table 3). The transition from colloform to spherulitic layers may be progressive, as illustrated in Fig. 7F. Relics of spherules within the colloform band "S1a" suggest that its massive character was acquired through progressive recrystallization (early burial diagenesis) of an initial spherulitic horizon. Contrary to this progressive transition, other transitions between spherulitic and colloform layers are distinctively sharp (e.g., limit "S1b"–"S2", Fig. 7G), and underlined by a distinct Al-silicate

(kaolinite?) rich lamina, clearly associated with a partial dissolution of the pre-existing sphalerite. The resulting voids are filled with a Fe–Mn calcite (0.8 to 1.9 wt.% Mn, 1.02 to 1.54 wt.% Fe; analyses SD2a-C1 and C4, Table 1). Sphalerite corrosion is testified by the irregular crenulated boundaries between the two co-existing mineral phases (Fig. 8E).

Galena layers (up to 1 mm thick: "G1" in Fig. 7B) consist of euhedral crystals (75 to 200 μm), often coalescing to form wider patches. Corroded boundaries between massive sphalerite "S1a" and galena "G1" (Fig. 8B) or "S2" and "G2" (Fig. 7B) are evidence that galena partially replaced previously-formed sphalerite and crystallized from the corroded boundaries toward the newly created discontinuity/void as euhedral to subhedral crystals. The bright μm-thick bands of galena along some weakness/discontinuity zones in the sphalerite spherules (Fig. 8A) are interpreted as replacement features, along with the small subhedral crystals (up to 40 μm though generally smaller) that overprint the concentric zoning within some spherules (Fig. 7E). Although galena consistently overprints sphalerite, there is considerable evidence of alternating episodes of galena or sphalerite growth. For instance, in the "G1" band, small sphalerite spherules (10 μm in diameter) occasionally fill voids within this galena layer, coating galena crystals. In the same way, the growth of the coarse galena crystals of the "G2" band was interrupted by the formation of a spherule lamina (Fig. 8D). Moreover, following the "G2" band, the alternation of galena and spherulitic sphalerite layers ("S3", "S4"; Fig. 8C, D) indicates an open-space filling. The remaining void was filled by (i) pyrite (see analysis SD2a-S17, Table 4) and (ii) an almost pure calcite (analysis SD2a-C5, Table 1; Fig. 7A, B). Eventually, after the late calcite void filling, sphalerite and galena were partly remobilized and fill microcracks in the calcite.
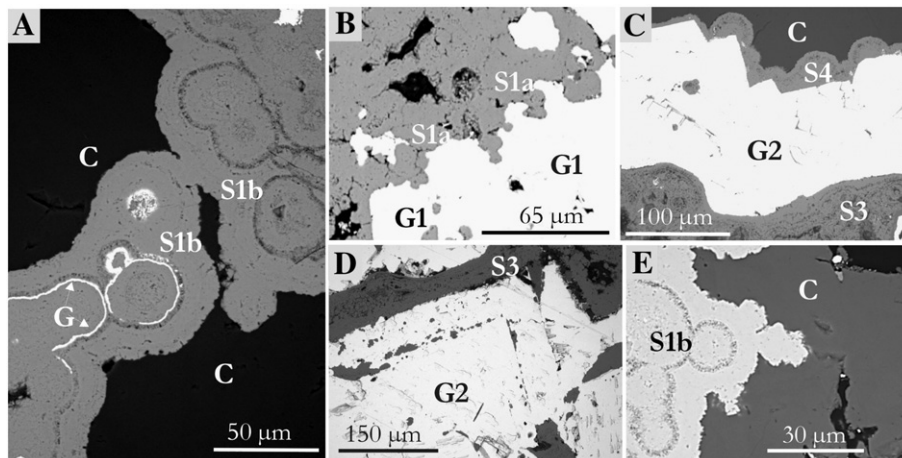

Fig. 8. Backscattered electron images of the banded ores from Sidi Driss (sample SD2a), where "C" is late calcite, "G1" and "G2" indicate two different galena layers and "S1a", "S1b", "S3" and "S4" four sphalerite layers. (A). Bright μm-thick bands of galena replacing growth zones in the sphalerite spherules of layer S1b. These spherules are surrounded by late calcite. (B). Corroded boundaries between the colloform sphalerite layer S1a and the galena layer G1, indicating replacement of sphalerite by galena. (C). Galena G2 growing on sphalerite spherules S3, and later covered by sphalerite spherules S4; S4 is the last sphalerite deposition episode before calcite void final infilling. (D). Galena crystal layer G2 exhibiting intergrowth with coeval sphalerite spherules. (E). Corroded boundaries between the sphalerite layer S1b and late calcite.

5.2.2. Sidi Driss barite-hosted mineralization

In the barite layers, sulfides are coeval with barite dissolution and partly replace the sulfate. Mineralization varies in style, from disseminated (Fig. 5H) to more massive (Fig. 5G, I). Galena was apparently the first sulfide to precipitate, roughly coating the rims of dissolution cavities within the barite matrix (Fig. 5J, H). Galena crystals (generally 10 to 100 μm, rarely larger) are usually euhedral to slightly subhedral, with minute outgrowth indicating the replacement of barite by the sulfide (Fig. 5J). In the disseminated ore, a Pb-sulfate (anglesite) often rims these outgrowths (Fig. 5J).

The dissolution cavities are filled either by a second barite generation (Ba2), defining the disseminated style (Fig. 5H) or by sulfides (sphalerite, marcasite), silicates (glauconite, quartz) and pure calcite, defining the more massive style (Fig. 5G). In the disseminated ore, galena growth was interrupted by coatings of sphalerite spherules (up to 15 μm, Fe-poor, up to 0.79 wt.% Cd, analysis SD2-S5, Table 3). These spherules are identical to those in the carbonate host-rocks and are more or less replaced by galena (Fig. 5J). Small, ~15 μm pyrite cubes occasionally occur within the galena. In the more massive ore, sphalerite occurs as spherules or spherule aggregates (10 to 20 μm in diameter), either within the barite matrix, together with a few galena patches, or as coatings or fillings of the dissolution voids. The sphalerite is Cd-rich and Fe-poor (from 0.65 wt.% Cd and 1.67 wt.% Fe in the barite matrix, analysis SD5-S3, to 0.22 wt.% Cd and 0.55 wt.% Fe in the void fillings, analysis SD5-S6, Table 3). Within the barite matrix, occasional sphalerite microcracks are evidence for a late introduction of the sulfide. At the void rims, limited replacement of sphalerite by galena is sometimes visible. As in the carbonate-hosted mineralization, sphalerite spherules display internal zoning with intergrowth of an Al-rich silicate (likely, kaolinite), whereas in the void fillings the spherules are coeval with a fine-grained mixture of quartz, glauconite (38.56 wt.% SiO_2, 0.67 wt.%

TiO_2, 13.28 wt.% Al_2O_3, 9.63 wt.% FeO, 1.17 wt.% MgO, 0.26 wt.% CaO, 0.73 wt.% Na_2O and 2.88 wt.% K_2O) and euhedral pyrite. Although some dissolution cavities are completely filled by the sphalerite–silicate mixture, others show first a coating by a sphalerite layer, then the crystallization of marcasite (Fig. 5I), sometimes followed by calcite. Limited replacements of either galena or sphalerite by marcasite are seen at the void rims. Marcasite is characterized by low to significant As contents (<mdl to 0.55 ppm; analyses SD5-S7 and SD5-S11, Table 4). Calcite is enriched in Fe and Mn (1.66 to 3.34 and 0.77 to 1.62 wt.%, respectively; analyses SD5-C3 and C1, Table 1).

5.2.3. Douahria carbonate-hosted disseminated mineralization

Sphalerite occurs as disseminated spherules (10 to 30 μm), often aggregated (Fig. 6D), that may coalesce into wider patches (Fig. 6B) that are in turn connected by μm-scale colloform "cracks" to form amoeboid aggregates (Fig. 6B, C). As for the Sidi Driss sphalerite, the Douahria spherules exhibit an internal zoning with intergrowth of an Al-rich silicate (likely kaolinite), and may be more or less recrystallized (Fig. 6D). Sphalerite is Fe-poor (<mdl) and contains Cd, with quite constant compositions at the sample scale (analyses DSU7-S5 and S8: 0.10 and 0.11 wt.% Cd; analyses DSU6-S3 and S5: 0.45 and 0.38 wt.% Cd, Table 3).

Galena is the most abundant sulfide. It occurs as 30 to 100 μm-size, euhedral to subhedral crystals (Fig. 6B) that sometimes coalesce within the matrix to form wider patches that sometimes underline the laminated character of the carbonate host-rock. In some instances, galena seems to replace a spherule sphalerite network (Fig. 6A).

Marcasite is a late phase and replaces the carbonate matrix along linear tracks (pseudo-veins) and interconnected patches, starting from the pseudo-vein (Fig. 6E), and decreasing in abundance with distance. These patches are in part replacing earlier galena and (mainly) sphalerite aggregates, of which only a few spherules remain in the vicinity of the pseudo-vein (Fig. 6E),
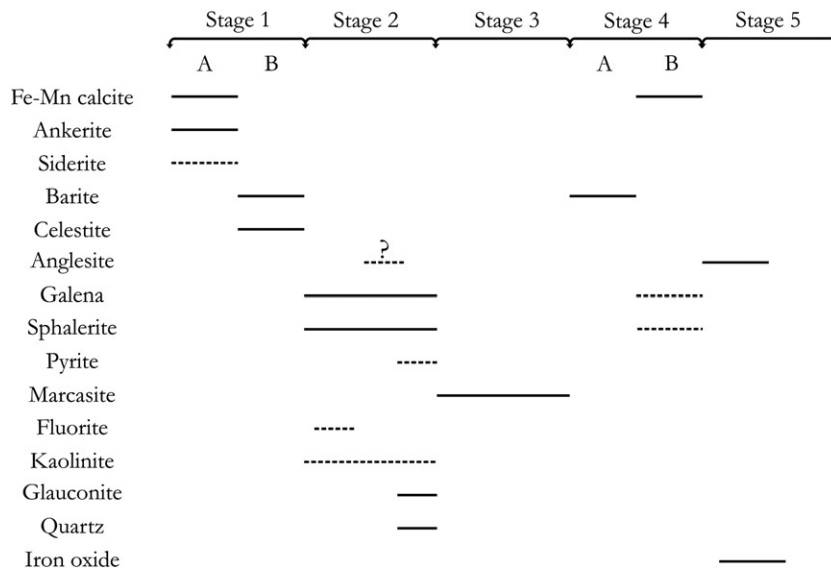

Fig. 9. Synthetic paragenetic sequence for the Sidi Driss and Douahria deposits. Recurrent mineral precipitation (e.g., sphalerite and galena alternations in sample SD2a) is grouped into a single paragenetic stage. Solid lines represent major minerals of a given stage and dashed lines represent accessory minerals. See text for further explanation.

whereas only partial replacement is observed further (Fig. 6D). Pure marcasite (analysis DSU7-S1, Table 4) characterizes the pseudo-vein, whereas in the replacement patches, marcasite is often As and Pb-bearing (0.64 and 1.54 wt.%, respectively, analysis DSU7-S4, Table 4).

The pseudo-veins exhibit vuggy parts (Fig. 6F), that are filled first by large euhedral Sr-poor barite (0.52 wt.%, analysis DSU7-C17, Table 2) laths (500 μm in length), then by pure sparry calcite (DSU7-C13, Table 1). Lath-shaped barite (20 μm in length) is also present as replacement in the carbonate rocks (Fig. 6B), being there clearly later than galena and sphalerite, and likely coeval with the pseudo-vein infillings. They are however variably enriched in Sr (from 0.48 wt.% to 4.41 wt.% Sr, DSU7-C20 and C18, Table 2).

5.2.4. Douahria celestite-hosted mineralization

Galena and hematite are the main minerals. Pure celestite layers alternate with partial replacement layers (a few mm in thickness), where galena surrounds and replaces the celestite crystals and Fe-oxides partially fill the porosity (Fig. 6G). Galena is partly oxidized and transformed into a Pb-sulfate (anglesite).

6. Paragenetic evolution

The preceding descriptions show that the mineral succession was identical in studied samples from the Sidi Driss and Douahria basins. That succession also appears to be independent of the host-rock (i.e., Fe–Mn calcites, barite, celestite). A single synthetic paragenetic sequence, subdivided into five stages of evolution, can consequently be defined for the two basins (Fig. 9).

- Stage 1 includes all the diagenetic transformations that affected the initial sediments before the inception of sulfide emplacement. Initially, the host-rocks for the mineralization were most probably dolomite Ca-sulfate sabkha/salina sediments developed at the expense of algal mats. Sub-stage 1A consisted of an early diagenetic dedolomitization process, involving Fe–Mn-enriched fluids, as testified by the co-existence of pure calcite, Fe–Mn bearing calcite, ankerite and, to a lesser extent, siderite in the dedolomitization products. Based on the observations in Dermech (1990), minerals of sub-stage 1A can be considered as present at the basin scale at Sidi Driss. Sub-stage 1B consisted of a partial to complete replacement of these early carbonates by sulfates, either celestite (Douahria) or barite±celestite (Sidi Driss).
- Stage 2 corresponds to the base metal mineralizing event. Galena and sphalerite (sometimes with limited pyrite at Douahria or accessory fluorite at Sidi Driss) were emplaced in the diagenetic carbonates and sulfates, through (1) matrix dissolution/replacement process or (2) void infilling. There is a systematic contrast between the habits of sphalerite (basically, spherulitic facies) and galena (euhedral cubes and cuboctaedra). Sphalerite deposition was consistently accompanied by subordinated silicates (kaolinite?, glauconite, quartz). Alternation of galena and sphalerite deposition was also systematic, although galena was often the first

sulfide in the sequence. Galena is frequently seen to replace sphalerite, but the opposite case is not observed.
- Stage 3 is characterized by Fe-sulfides (pyrite, marcasite, often As-bearing) that replace earlier carbonates and/or sulfides and fill voids.
- Stage 4 consists of late infilling of remaining voids by barite (sub-stage 4A) and (Fe–Mn) calcite (sub-stage 4B).
- Stage 5 corresponds to the oxidized assemblages. Development of anglesite at the expense of galena is the main process. It is better expressed at the Douahria deposit, where late crystallization of an iron oxide is also seen. The relationships between galena alteration and the iron oxides are not known, but they could have been coeval. Iron oxide precipitation was possibly related with the development of the overlying Tamra iron formation.

7. Sulfur isotopes

δ^{34}S data for sulfates display a wide range of positive δ^{34}S values from $+21.5$ to $+57.0‰$ (Table 5, Fig. 10). Two populations

Table 5
δ^{34}S values of sulfate, galena and Fe-sulfides from the Sidi Driss and Douahria ore deposits

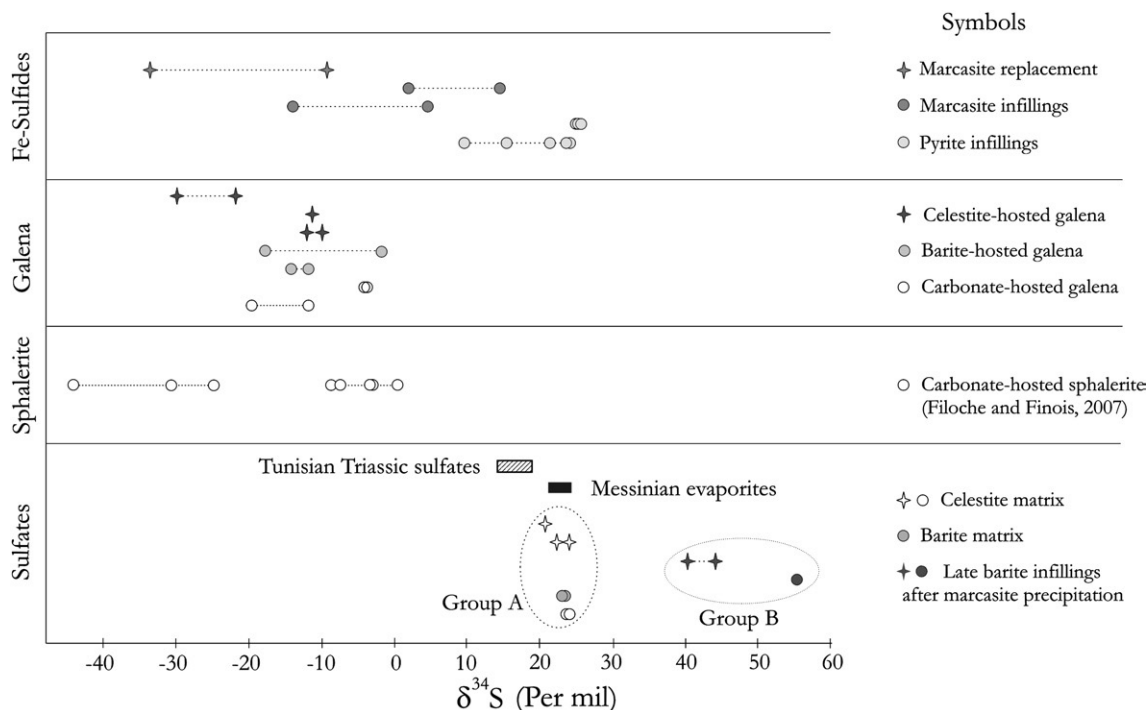| Mineral	Mine	Sample	δ^{34}S (‰)
Barite	Sidi Driss	SD2	23.5
			22.9
		pyr1	57.0
	Douahria	DSU7	40.7
			43.9
Celestite	Sidi Driss	BXW	24.4
			23.6
	Douahria	DSU2	23.7
			22.6
		DSU3	21.5
Galena	Sidi Driss	SD2a	−2.0
			−18.1
		CI3	−13.5
			−12.2
		SD5	−3.7
			−4.0
		SD2	−12.2
			−18.7
	Douahria	DSU2	−10.6
		DSU4	−21.7
			−30.3
		DSU5	−11.7
			−9.9
Fe-sulfides	Sidi Driss	SD2a	9.0
			23.6
			15.7
			21.4
			23.7
		SD5	−14.2
			4.2
		pyr1	12.1
			1.9
		pyr2	25.8
			25.8
			25.0
	Douahria	DSU7	−35.9
			−8.7

Fig. 10. δ^{34}S isotopic values of sulfates (barite and celestite), galena and Fe-sulfides from the Sidi Driss and Douahria deposits. Stars correspond to Douahria samples and circles are for Sidi Driss samples. Data for Messinian evaporites were taken from Claypool et al. (1980) and Paytan et al. (1998), and data for Triassic sulfates from Tunisia were taken from Sheppard et al. (1996). Group A corresponds to the celestite and barite matrix of sub-stage 1B and group B includes the late barites of sub-stage 4A.

may be identified. A first group (Group A in Fig. 10) corresponds to the celestite and barite matrix of sub-stage 1B and exhibits δ^{34}S values from +21.5 to +24.4‰. These values are in the range of Messinian evaporites (+20.7 to +24‰; Claypool et al., 1980), which is consistent with the conclusion of the preceding section where the sulfates are considered derived Messinian Ca-sulfates. The second group (Group B in Fig. 10) includes the late barites of sub-stage 4A and is characterized by the highest δ^{34}S values (from +40.7 to +57.0‰).

All the δ^{34}S values for galena are negative, with a wide range from −30.3 to −2.0‰ (Fig. 10). At the crystal scale, the δ^{34}S are either nearly constant or strongly variable (Fig. 10). There is no clear relationship between the sulfur isotope signatures and nature of the host matrix (sulfate, carbonate) and/or the mode of emplacement of the galena (replacement or infilling). However, there is a slight tendency towards lower δ^{34}S in galena from Douahria.

The Fe-sulfides display a still larger variability than galena, with δ^{34}S ranging from −35.9 to +25.8‰ (Fig. 10). δ^{34}S is usually variable within a single crystal, while it remains constant in one Sidi Driss pyrite. The late pyrite infillings in Sidi Driss exhibit higher δ^{34}S values (from +9.0 to +25.8‰) than the marcasites from both Douahria and Sidi Driss (from −35.9 to +16.8‰). As for the galenas, there is a slight tendency towards lower δ^{34}S for in marcasite from Douahria.

Preliminary *in situ* measurements for δ^{34}S in sphalerite spherule aggregates from Sidi Driss (Filoche and Filinois, 2007) yielded both strong negative values (from −24.7 down to −43.9‰) and more positive values (−8.1 to +1.2‰).

8. Discussion

8.1. Sulfur source(s)

There is considerable evidence for replacement of the early barite or celestite by sphalerite or galena. This strongly suggests that these sulfates could have been, at least partly, a sulfur source for the sulfides within the sulfate-hosted mineralization in the studied basins. As mentioned above, the group A barites and celestites display δ^{34}S in the range +21.5 to +24.4‰, consistent with contemporaneous (Messinian) seawater (δ^{34}S=+20.7 to +24‰; Claypool et al., 1980). In the carbonate-hosted mineralization, the early sulfides could have also replaced earlier sulfate or, alternatively, have taken directly their sulfur from Messinian seawater. A deeper source of sulfate sulfur (namely, Triassic sulfates from, for instance, the Oued Belif diapir) must, however, also be considered. Since it is known that brines are the only way to efficiently transport Pb and Zn in hydrothermal solution (e.g., Hanor, 1996), a brine source is needed in the Sidi Driss and Douahria cases. The Triassic evaporites are the only reasonable source of brines in northern Tunisia, where significant Messinian evaporite deposits are unknown. In Tunisia, the δ^{34}S from diapir anhydrite cap-rocks is typically of 16‰ (Charef and Sheppard, 1991).

A sulfide source of sulfur could also be considered. Indeed, in the northern Tunisia autochthonous series, the Cenomanian–Turonian Bahloul Formation (which otherwise constitutes a major aquifer; Orgeval et al., 1986) is part of a worldwide anoxic event and is strongly enriched in diagenetic pyrite, the leaching of which would provide a significant source of reduced

sulfur. Although there are no available $\delta^{34}S$ data for pyrite from the Bahloul Formation, it is well known that pyrite from this event is universally characterized by very low $\delta^{34}S$ values (≤ -20‰; Ohkouchi et al., 1999).

Sulfate reduction leads to important sulfur isotopic fractionation, the extent of which strongly depends upon the reducing agent and the characteristics of the local environment (i.e., open vs. closed system; Ohmoto, 1986). Two processes may be considered (Machel, 2001; Peevler et al., 2003 and references therein): a low-temperature bacterially-mediated reduction process (BSR) and a thermally-driven abiotic chemical reduction process (TSR). We now discuss in more details the sulfur source problem for the different minerals.

The microspherulitic texture of *sphalerite* is reminiscent of a biomineralization processes resulting from BSR, as observed in the Tennyson Pb–Zn mine wastes, Wisconsin (Labrenz et al., 2000) or the Hazlehurst salt dome, Missouri (Southam and Saunders, 2005). Similar textures were also observed in the Carnian Bleiberg Zn–Pb deposit, Austria, and are interpreted as resulting from a BSR process involving Carnian sulfates, based on the low (-30‰) $\delta^{34}S$ in the sphalerite (Schroll and Rantisch, 2003). In an open system, BSR results in ^{34}S fractionations of $\Delta^{34}S \gg -20$‰ according to Machel (2001). Consequently, the strongly negative $\delta^{34}S$ values measured in the Sidi Driss sphalerite microspherules (from -24.7 down to -43.9‰) are consistent with BSR. These microspherules could result from a biomineralization, provided that the source sulfate had the $\delta^{34}S$ of Messinian (or, possibly, Triassic) sulfates. In their study of the Bou Grine Pb–Zn ore deposit, however, Bechtel et al. (1996) cogently underlined that BSR fractionation also depends upon sulfate availability. In closed systems, where sulfate supply is limited (though still open for H_2S), less fractionated $\delta^{34}S$ values are obtained through the BSR process, and the enrichment may reach 40‰ (Ohmoto, 1986). Such a possibility could explain the less negative $\delta^{34}S$ values measured in some sphalerite microspherules (from -8.1 to $+1.2$‰).

The same line of reasoning could also apply to *galena*, with $\delta^{34}S$ between -30 and -2‰. Nevertheless, several lines of evidence seem to contradict with the BSR hypothesis with respect to galena. Firstly, BSR-linked galena always displays characteristic textures (skeletal, framboidal, etc.) – e.g., at Navan, Ireland (Fallick et al., 2001) or at Bleiberg, Austria (Schroll, 1996) – that were not observed in the Sidi Driss and Douahria deposits. Moreover, at Navan and Bleiberg, galena and sphalerite record recurrent and systematic intergrowth, which is not the case at Sidi Driss and Douahria, where galena usually replaces sphalerite (the reverse is never observed). Secondly, galena in the Tunisian sites has often grown following dissolution of either sulfate or sphalerite, with euhedral habits testifying to open-space crystallization (e.g., Fig. 6B). In such a case, closed system crystallization is obviously possible, though less probable. Given the permeability increase associated with the dissolution event, renewal of the feeding hydrothermal solutions is likely. It is not irrelevant to note that similar situations have been reported from other deposits. For instance, at Navan, Ireland (Fallick et al., 2001), where most sulfides (including galena) are crystallized through BSR, an independent

galena generation is observed (expressed as large bladed crystals in void fillings) that displays heavier sulfur than the other sulfides. This heavy sulfur is thought to originate in a "deep" hydrothermal reservoir, an explanation that could hold as well for Sidi Driss and Douahria. On the other hand, the very light sulfur ($\delta^{34}S$ down to -30‰) measured in some galena crystals from Sidi Driss and Douahria does not necessary imply the involvement of a BSR process. Since most of the sphalerite is characterized by low $\delta^{34}S$ values (< -25‰), and galena is frequently observed replacing sphalerite, inheritance of a light sulfur component in the building of the overprinting galena seems unavoidable. On a textural basis, it seems difficult to explain the rather heavy sulfur found in most of the Sidi Driss and Douahria galena using the "closed system" version of the BSR process. The wide range of $\delta^{34}S$ values (-30 to -2‰) in our galena should be best explained by the mixing of an independent source of heavy sulfur with the light sulfur inherited from the dissolution of pre-existing sphalerite.

Three possibilities must be considered for the source of this "heavy" sulfur component. First, reduced sulfur could be provided by a deep reservoir, such as the diagenetic pyrites from the Bahloul Formation. Unfortunately, as mentioned before, the $\delta^{34}S$ of such pyrites (≤ -20‰) is probably too low to be the sulfur source for our galena. Second, heavy sulfur could have been produced at depth by TSR from the Triassic sulfates, as proposed for several northern Tunisia diapir-related Pb–Zn deposits, in which $\delta^{34}S$ typically ranges between -15 and 30‰ (mostly positive) (e.g., Sheppard and Charef, 1990; Charef and Sheppard, 1991; Orgeval, 1994; Bechtel et al., 1996). It has been proposed that this (dominantly) "heavy" sulfur was related to fault-leaked H_2S produced by TSR at high temperature, from mature oil and gas reservoirs at depth (e.g., Bechtel et al., 1996 and references therein) and was subsequently mixed with other sources of lighter sulfur, involving BSR (e.g., Sheppard et al., 1996). Such a deep-seated source of "heavy" sulfur should be considered for the Sidi Driss and Douahria galenas as well, and could be sought in the root of the nearby Oued Belif diapir. Yet, the Sidi Driss and Douahria galenas never yield as positive $\delta^{34}S$ values as the diapir-related galenas. Third, the "heavy" sulfur could have been produced by TSR *in situ*, from the Messinian sulfates. This would have been possible, for instance, if warm CH_4-bearing hydrothermal fluids had invaded the Messinian aquifers. Moreover, since sulfates are present in the deposit setting, it is logical to seek a local source of sulfur, especially as galena is often found to replace sulfates. According to Machel (2001), the TSR fractionation results in $\Delta S \geq -20$‰. Thus, starting from Messinian (or even, Triassic) $\delta^{34}S$ sulfate values, the highest $\delta^{34}S$ values observed in the Sidi Driss and Douahria galenas could easily be obtained through TSR.

Finally, we conclude that the range in $\delta^{34}S$ compositions measured in the Sidi Driss and Douahria galena is best explained by a mixing process between "light" inherited sulfur (evolved by BSR) and "heavy" pristine sulfur. The latter could have been generated at depth, through TSR at the expense of Triassic sulfate, but we rather favor an *in situ* origin, through TSR starting from either the Messinian sulfates or leached sulfate ions deriving from underlying Triassic evaporites, or

(most likely) both sources. Preliminary microthermometric study of primary fluid inclusions in late calcite from Sidi Driss (see below) clearly supports this hypothesis.

Since sphalerite and galena are often replaced by marcasite, the preceding explanation about inheriting of replaced sulfide signatures might hold also for the wide range of measured $\delta^{34}S$ values in marcasite (Fig. 10). On the other hand, largely positive $\delta^{34}S$ values observed in some marcasite and in the late pyrite infillings cannot be explained by this mechanism. A non-fractionated contribution of stage 1B sulfates (barite and/or celestite) could explain values clustering around +23‰. In this case, the available sulfates would have been completely consumed by marcasite (as suggested for pyrite in a comparable case by Machel et al., 1995). There is no evidence, however, of earlier sulfate in the cavities presently occupied by the marcasite under discussion. Our preferred explanation is a Rayleigh fractionation process in a closed system, where early sulfide precipitations are strongly enriched in ^{32}S and later "residual" sulfides are subsequently ^{34}S-enriched. The same fractionation process in a closed system can readily explain the late heavily fractionated barite ($\delta^{34}S$ values from +40.7 to +57.0‰, group B, Fig. 10), following a major loss of light ^{32}S through precipitation of Fe-sulfides ($\delta^{34}S = -35.9$ to +12.1‰).

8.2. Consequences for the hydrothermal system(s)

Our favored model for the source of sulfur has strong implications regarding the temperature of ore formation. On one hand, according to Machel (2001), the BSR process usually occurs at temperatures below 80 °C, even if hyperthermophilic sulfate-reducing bacteria can live at temperatures as high as ~110 °C, thus constraining the sphalerite deposition temperature to low (<80–(100)°C) values. This is consistent with the low Fe contents in the sphalerite. On the other hand, TSR typically involves high temperatures, >100 °C in any case, and more to be efficient (Machel, 2001). Thus, whether the "heavy" sulfur was produced at depth or in situ, our favored model implies involvement of a warm hydrothermal fluid for the galena crystallization. This is consistent with the frequent replacement of sphalerite by galena, since experimental data indicate an inversion in the solubility of these two sulfides at around 150 °C (Barrett and Anderson, 1988; Seward and Barnes, 1997).

There is some evidence to reinforce these conjectural views. Firstly, using ^{18}O data, Dermech (1990) estimated the crystallization temperatures of the (early) Fe–Mn carbonates at Sidi Driss between 70 and 100 °C, consistent with the BSR process at the origin of the subsequent sphalerite. Second, our preliminary microthermometric study of primary fluid inclusions in the late calcite from the SD04/5 sample (stage 4B, Fig. 9) yielded the following results: high salinity (11.7 to 18.3 wt.% NaCl equiv.) in the NaCl–H_2O system; Th between 160 and 190 °C. This hot brine is thought to be a late representative of the warm fluids involved in our model.

8.3. Early character of the mineralizations

Several lines of reasoning argue for the Sidi Driss and Douahria Pb–Zn deposits being emplaced during diagenesis of

the carbonate sediments: (i) Fe–Mn enrichments in the early diagenetic carbonates imply inception of hydrothermal circulation since this early stage, (ii) sulfur isotope data for galena suggest involvement of Messinian seawater, (iii) the Pb–Zn-sulfides were deposited at low temperatures, and (iv) 'soft'-style sedimentary figures in the banded ores at Sidi Driss are evidence for syn-compactional deposition.

Consequently, the Sidi Driss and Douahria Pb–Zn deposits are better classified as sediment-hosted massive sulfides (SHMS) than as Mississippi Valley Type (MVT) deposits, notwithstanding the replacement/dissolution features exhibited by the disseminated ores. By some aspects, the studied deposits are very similar to sedimentary exhalative (Sedex) deposits: (i) early Fe–Mn carbonates, the repartition of which is larger than that of the base metal sulfides, as in the Proterozoic Australian Sedex deposits (Large and McGoldrick, 1998); (ii) barite deposition preceding base metal sulfides and the diagenetic sulfates being a source of sulfur, as in the Red Dog deposit, Alaska (Kelley et al., 2004) and (iii) Cd enrichment in sphalerite (Piatak, 2004). Of course, the Sidi Driss and Douahria Pb–Zn deposits differ from the usual Sedex by their very low metal tonnage. This implies that the limiting factor in the Sidi Driss and Douahria mineral deposits was not the availability in sulfur, as in many hydrothermal deposits, but the availability in base metals (or, their equivalent in terms of inflowing metal-bearing fluid). Indeed, remaining sulfates testify to the fact that the sulfate reduction and metal sulfide precipitation only consumed a restricted part of the available sulfur stock in the basin.

8.4. Genetic modeling

The Southern Tunisian MVT deposits are diapir-related (Rouvier et al., 1985). Although part of the Pb–Zn concentrations may be earlier than the Late Neogene (as advocated for the Bou Grine deposit, which could belong to the SEDEX class: Charef and Sheppard, 1991; see also Sheppard et al., 1996), there is much evidence for a Late Neogene deposition stage (Perthuisot and Rouvier, 1996). Therefore, a significant part of these MVT mineralizations may be interpreted as the result of a gravity-driven fluid circulation event related to late Alpine convergence and thrust sheet formation in the Maghrebides (Kyle and Posey, 1991; Perthuisot and Rouvier, 1996). Meteoric fluids infiltrated in the Alpine highlands to the north are thought to have circulated in deep aquifers from the external zones and risen along southernmost thrusts and associated diapirs, where they deposited Pb- and Zn-sulfides (Fig. 11). This is a classical process in the fold-and-thrust belts forelands elsewhere (e.g., Bradley and Leach, 2003). The timing of this major hydrothermal event is poorly constrained at the deposit scale. However, since the late Alpine convergence occurred in Tunisia during the Late Serravallian–early Tortonian times (Bouaziz et al., 2002), inception of the topographically-driven hydrothermal system is likely to have occurred during the Serravallian–Tortonian (Fig. 11). The syn-diagenetic Sidi Driss and Douahria deposits cannot be related to this circulation event for the following reasons: (i) they are apparently younger (Messinian in age) than the MVT deposits, (ii) they are hosted in
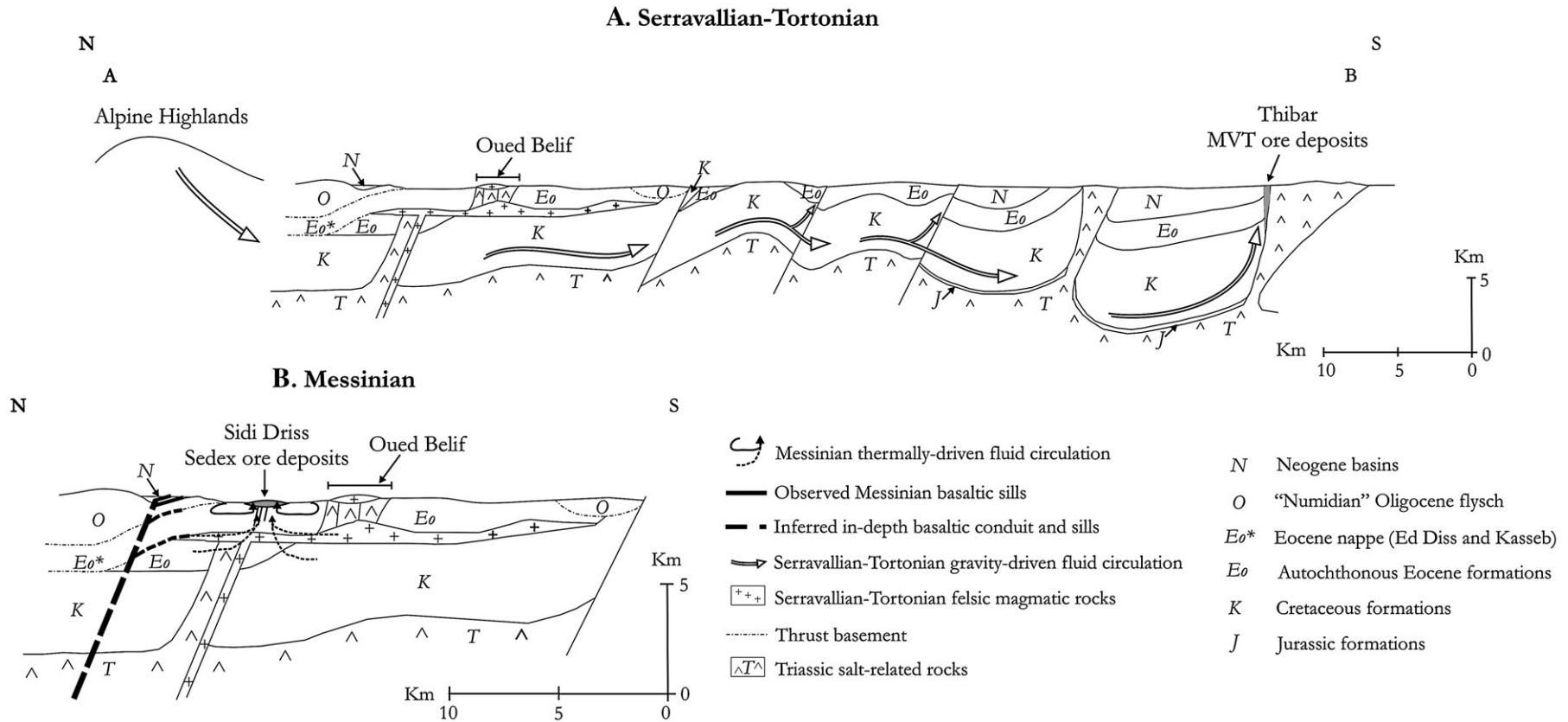
Fig. 11. Synthetic and schematic geological cross-sections at the basin scale (see Fig. 1 for location), illustrating likely circulation of mineralizing fluid. (A) Gravity-driven circulation leading to formation of typical MVT Pb–Zn ore deposits (e.g., Thibar) during the Serravallian–Tortonian. (B) Thermally-driven circulation involved in formation of Sedex type Pb–Zn deposits (e.g., Sidi Driss) during Messinian (after Rouvier, 1977, Perthuisot, 1981, Rouvier et al., 1985, Ben Ferjani et al., 1990, Perthuisot and Rouvier, 1992, and Jallouli et al., 2003).

small post-convergence extensional basins, and (iii) their low tonnage apparently precludes the involvement of a large hydrothermal system.

On the other hand, thermal anomalies are known in the Nefza region since Late Serravallian–Tortonian times (e.g., Oued Belif intrusions) and are still present (active Nefza hydrothermalism; Zouiten (1999) and regional high thermal gradient going over 10 °C/100 m; Jallouli et al., 1996). A direct genetic relationship between the Serravallian–Tortonian Oued Belif magmatism and the Sidi Driss deposit, as proposed by Dermech (1990), cannot hold, due to the Messinian age of both the mineralization host-rock and the ore deposit it contains. By contrast, a link with the Messinian mafic magmatism recorded in the Nefza region (Rouvier, 1994 and references therein) can be proposed and is consistent with the extensional conditions recorded at that time in northern Tunisia (Bouaziz et al., 2002). This, together with a possible/probable role of a shallow concealed magmatic sill (Jallouli et al., 2003), would allow for the development of small, shallow convection cells, providing the source for the higher temperature (≥ 150 °C) fluids involved in the thermochemical reduction of sulfates, at the site of galena deposition.

The Sidi Driss and Douahria ores would find their origin in the mixing of "deep" and shallow-basinal fluids, thus explaining the temperature fluctuations recorded by the alternating deposition of BSR (sphalerite) and TSR (galena) related sulfides (Fig. 11). The circulation of these mixed origin fluids through the permeable levels in the basins (i.e., carbonates), was likely driven and forced by the high Messinian geothermal gradients. Structural discontinuities (thrust sheet boundaries, magmatic contacts, and deformed diapirs) likely served as the main fluid conduits. In particular, the longitudinal NE-SW faults underneath the Sidi Driss basin apparently forced the fluids upwards into the permeable levels of the basin (Dermech, 1990), and were the host for the small Pb–Zn veins in the Eocene basement of the Sidi Driss basin (Ed Diss nappe). Leaching of felsic magmatic rocks may have contributed to the base metal enrichment and are the likely source for the fluorine (as fluorite) in the Sidi Driss disseminated ores.

9. Conclusions

Textural, geochemical and isotopic studies of the Sidi Driss and Douahria ores have shown the complex and multi-stage nature of these occurrences and their early/syn-diagenetic (Messinian) character. Notwithstanding the replacement/dissolution features exhibited by the ores, several geometric and geochemical properties of the Sidi Driss and Douahria occurrences favor their classification as SHMS-Sedex ore deposits, with early sulfates and Messinian seawater as the major sulfur source. The wide range of $\delta^{34}S$ values measured in sphalerite, galena and Fe-sulfides is interpreted as the result of (i) alternating BSR and TSR fractionation, and (ii) sulfur inheritance through replacement, at poorly constrained, though generally low, fluctuating temperatures.

However, these deposits differ from the usual Sedex type by their very low metal tonnage, which excludes involvement of a large hydrothermal system. In the Sidi Driss and Douahria ore

deposits, the limiting factor was not the availability of sulfur, as in many hydrothermal deposits, but the availability of base metals. The latter were probably leached from either the older Serravallian–Tortonian felsic magmatic bodies (shallow intrusion) or the Triassic evaporites from the Oued Belif diapir (or both); both units are of limited geographical extent.

We favor a hypothesis of small-scale shallow convection cells driven by high geothermal gradients during the Messinian, as suggested by the mafic magmatism and the extensional conditions recorded for that period in northern Tunisia (Bouaziz et al., 2002). Such sulfide emplacement is significantly different from that of the MVT ore deposits to the south that are associated with diapirs and which are interpreted as the result of a Serravallian–Tortonian gravity-driven fluid circulation event (Kyle and Posey, 1991; Perthuisot and Rouvier, 1996), related to late Alpine convergence.

References

Aïssa, D., Marignac, Ch., Cheilletz, A., Gasquet, D., 1998. Géologie et métallogénie sommaire du massif de l'Edough (NE Algérie). Mémoires du Service Géologique de l'Algérie n°9, 7–55.

Barrett, T., Anderson, G., 1988. The solubility of sphalerite and galena in 1–5 m NaCl solutions to 300 °C. Geochimica et Cosmochimica Acta 52, 813–820.

Bechtel, A., Shieh, Y.-N., Pervaz, M., Püttmann, W., 1996. Biodegradation of hydrocarbons and biogeochemical sulfur cycling in the salt dome environment: inferences from sulfur isotope and organic geochemical investigations of the Bahloul Formation at the Bou Grine Zn/Pb ore deposit, Tunisia. Geochimica et Cosmochimica Acta 60, 2833–2855.

Bellon, H., 1976. Séries magmatiques néogènes et quaternaires du pourtour de la Méditerranée occidentale, comparées dans leur cadre géochronologique; implications géodynamiques. Unpublished Ph.D. Thesis, Paris South University, France, 367 pp.

Ben Ferjani, A., Burollet, P., Mejri, F., 1990. Petroleum geology of Tunisia. Entreprise Tunisienne d'Activités Pétrolières. Tunis. 194 pp.

Berthon, L., 1922. L'industrie minérale en Tunisie. Service des Mines de Tunisie. 272 pp.

Bouaziz, S., Barrier, E., Soussi, M., Turki, M.M., Zouari, H., 2002. Tectonic evolution of the northern African margin in Tunisia from paleostress data and sedimentary record. Tectonophysics 357, 227–253.

Bradley, D.C., Leach, D.L., 2003. Tectonic controls of Mississippi Valley-type lead–zinc mineralization in orogenic forelands. Mineralium Deposita 38, 652–667.

Callot, J.P., Jahani, S., Letouzey, J., Sherkati, S., 2005. The role of pre-existing diapirs in fold and thrust belt development. In: Lacombe, O., Lavé, J., Roure, F., Vergès, J. (Eds.), Thrust Belts and Foreland Basins, International Meeting, Rueil-Malmaison (France), Abstract Volume, pp. 82–85.

Charef, A., Sheppard, S.M.F., 1991. The diapir related Bou Grine Pb–Zn deposit (Tunisia): evidence for role of hot sedimentary basin brines. In: Pagel, M., Leroy, J. (Eds.), Source, Transport and Deposition of Metals. Balkema, Rotterdam, pp. 269–272.

Claypool, G., Holser, W., Kaplan, I., Sakai, H., Zak, I., 1980. The age curves of sulfur and oxygen isotopes in marine sulfate and their mutual interpretation. Chemical Geology 28, 199–260.

Crampon, N., 1971. Etude géologique de la bordure des Mogods, du pays de Bizerte et du nord des Hédil. Unpublished Ph.D. thesis, Nancy I University, France, 522 pp.

Decrée, S., De Putter, Th., Yans, J., Recourt, Ph., Jamoussi, F., Bruyère, D., Dupuis, Ch., in press. Iron mineralization in Pliocene sediments of the Tamra iron mine (Nefza mining district, Tunisia): mixed influence of pedogenesis and hydrothermal alteration. Ore Geology Reviews. doi:10.1016/j.oregeorev.2007.02.001.

Dermech, M., 1990. Le complexe de l'Oued Bélif - Sidi Driss (Tunisie septentrionale). Hydrothermalisme et métallogénie. Unpublished PhD thesis, Paris VI University, France, 336 pp.

El Bakkali, S., Bourdier, J.-L., Gourgaud, A., 1998. Caractérisation et stratigraphie de dépôts volcanoclastiques marqueurs dans le Miocène supérieur du bassin de Melilla-bas Kert (Rif oriental, Maroc). Comptes-Rendus de l'Académie des Sciences de Paris 327, 93–100.

Fallick, A.E., Ashton, J.H., Boyce, A.J., Ellam, R.M., Russell, M.J., 2001. Bacteria were responsible for the magnitude of the world-class hydrothermal base metal sulfide orebody at Navan, Ireland. Economic Geology 96, 885–890.

Faul, H., Foland, K., 1980. L'âge des rhyodacites de Nefza-Sedjenane. Notes du Service Géologique de Tunisie n°46. Travaux de Géologie Tunisienne, vol. 14, pp. 47–49.

Filoche, C., Flinois, J.S., 2007. Interférence de la réduction bactérienne des sulfates (BSR) et de la thermoréduction chimique (TSR) dans le cas d'une minéralisation sédimentaire de Zn–Pb (Sidi Driss, Tunisie): test par l'analyse isotopique du soufre par microsonde ionique. Unpublished Bachelor's thesis INPL-Nancy, 31 pp.

Gottis, Ch., Sainfeld, P., 1952. Les gîtes métallifères tunisiens. XIXème Congrès Géologique International. Monographies régionales, 2e série: Tunisie - n°2. 104 pp.

Hanor, J.S., 1996. Controls on the solubilization of lead and zinc in basinal brines. In: Sangster, D.F. (Ed.), Carbonate-hosted lead–zinc deposits, 4. SEG Special Publications, pp. 483–500.

Jaeger, J.-J., 1977. Les rongeurs du Miocène moyen et supérieur du Maghreb. Palaeovertebrata 8 (1), 1–166.

Jallouli, C., Inoubli, M.H., Albouy, Y.Y., 1996. Le corps igné de Nefza (Tunisie septentrionale): caractéristiques géophysiques et discussion du mécanisme de sa mise en place. Notes du service Géologique de Tunisie n°62, pp. 109–123.

Jallouli, C., Mickus, K., Turki, M.M., Rihane, C., 2003. Gravity and aeromagnetic constraints on the extent of Cenozoic rocks within the Nefza–Tabarka region, northwestern Tunisia. Journal of Volcanology and Geothermal Research 122, 51–68.

Kelley, K., Leach, D., Johnson, C., Clark, J., Fayek, L., Slack, J., Anderson, V., Ayuso, R., Ridley, W., 2004. Textural, compositional, and sulfur isotope variations of sulfide minerals in the Red Dog Zn–Pb–Ag deposits, Brooks Range, Alaska: implications for ore formation. Economic Geology 99, 1509–1532.

Kyle, J., Posey, H., 1991. Halokinesis, cap rock development, and salt dome mineral resources. In: Melvin, J. (Ed.), Evaporites, Petroleum and Mineral Resources. Elsevier, Amsterdam, pp. 445–469.

Labrenz, M., Druschel, G.K., Thomsen-Ebert, T., Gilbert, B., Welch, S.A., Kemner, K.M., Logan, G.A., Summons, R.E., De Stasio, G., Bond, P.L., Lai, B., Kelly, S.D., Banfield, J.F., 2000. Sphalerite (ZnS) deposits forming in natural biofilms of sulfate-reducing bacteria. Science 290, 1744–1747.

Large, R., McGoldrick, P., 1998. Lithogeochemical halos and geochemical vectors to stratiform sediment hosted Zn–Pb–Ag deposits. Part 1: Lady Loretta deposit, Queensland. Journal of Geochemical Exploration 63, 37–56.

Machel, H., 2001. Bacterial and thermochemical sulfate reduction in diagenetic settings — old and new insights. Sedimentary Geology 140, 143–175.

Machel, H., Krouse, H., Sassen, R., 1995. Products and distinguishing criteria of bacterial and thermochemical sulfate reduction. Applied Geochemistry 10, 373–389.

Marignac, C., 1988. A case of ore deposition associated with geothermal activity: the polymetallic ore veins of Aïn Barbar (NE Constantinois, Algeria). Mineralogy and Petrology 39, 107–127.

Mauduit, F., 1978. Le volcanisme néogène de la Tunisie continentale. Unpublished Ph.D. thesis, Paris South University, France, 157 pp.

Negra, L., 1987. Pétrologie, minéralogie et géochimie des minéralisations et des roches encaissantes des basins associés aux structures tectoniques et magmatiques de l'Oued Bélif et du Jebel Haddada (Nord des Nefza, Tunisie septentrionale). Unpublished Ph.D. thesis, Paris-Sud University, France, 223 pp.

Ohkouchi, N., Kawamura, K., Kajiwara, Y., Wada, E., Okada, M., Kanamatsu, P., Taira, A., 1999. Sulfur isotope records around Livello–Bonarelli (northern Apennines, Italy) black shale at the Cenomanian–Turonian boundary. Geology 27, 535–538.

Ohmoto, H., 1986. Stable isotope geochemistry of ore deposits. In: Valley, J.W.R., Taylor, H.P., O'Neill, J.R. (Eds.), Stable isotopes in high temperature geological processes. Reviews in Mineralogy, vol. 16, pp. 491–599.

Orgeval, J.J., 1994. Peridiapiric metal concentration: example of the Bou Grine deposit (Tunisian Atlas). In: Fontbote, L., Boni, M. (Eds.), Sediment-hosted Zn–Pb ores. SGA Special Publication, vol. 10. Springer-Verlag, Berlin-Heidelberg, pp. 354–389.

Orgeval, J.J., Giot, D., Karoui, J., Monthel, J., Sahli, R., 1986. Le gisement de Zn–Pb de Bou Grine (Atlas tunisien). Description et historique de la découverte. Chronique de la Recherche Minière 482, 5–32.

Paytan, A., Kastner, M., Campbell, D., Thielmens, M., 1998. Sulfur isotopic composition of Cenozoic seawater sulfate. Science 282, 1459–1462.

Peevler, J., Fayek, M., Misra, K.C., Riciputi, L.R., 2003. Sulfur isotope microanalysis of sphalerite by SIMS: constraints on the genesis of Mississippi Valley Type mineralization, from the Mascot–Jefferson City District, East Tennessee. Journal of Geochemical Exploration 80, 277–296.

Perthuisot, V., 1981. Diapirism in northern Tunisia. Journal of Structural Geology 3, 231–235.

Perthuisot, V., Rouvier, H., 1992. Les diapirs du Maghreb central et oriental: des appareils variés, résultats d'une évolution structurale et pédogénétique complexe. Bulletin de la Société Géologique de France 163, 751–760.

Perthuisot, V., Rouvier, H., 1996. Les dépôts Pb–Zn associés aux évaporites du Trias des diapirs du Maghreb oriental (Tunisie). 16ème Réunion des Sciences de la Terre, Orléans. Société Géologique de France, Paris, p. 158.

Piatak, N., 2004. Environmental significance of cadmium and other trace-element concentrations in sphalerite from mineral deposits. Geological Society of America, Abstracts with Program, vol. 36(5), p. 27.

Roman, F., Solignac, M., 1934. Découverte d'un gisement de Mammifères pontiens à Douaria (Tunisie septentrionale). Comptes-Rendus de l'Académie des Sciences de Paris 199, 1649–1659.

Rouvier, H., 1977. Géologie de l'extrême Nord Tunisien: tectonique et paléogéographie superposées à l'extrémité orientale de la chaîne Nord-Maghrebine. Unpublished Ph.D. thesis, Pierre et Marie Curie University, Paris, France, 215 pp.

Rouvier, H., 1987. Carte géologique de la Tunisie; feuille n°10: Nefza. Service Géologique, Office National des Mines.

Rouvier, H., 1994. Notice explicative de la carte géologique de la Tunisie au 1/50000e - Nefza, feuille 10. Office National des Mines, Direction de la Géologie. 48 pp.

Rouvier, H., Perthuisot, V., Mansouri, A., 1985. Pb–Zn deposits and salt-bearing diapirs in Southern Europe and North Africa. Economic Geology 80, 666–687.

Sainfeld, P., 1952. Les gîtes plombo-zincifères de Tunisie. Annales des Mines et de la Géologie 9, 285.

Sanz-Rubio, E., Sánchez-Moral, S., Cañaveras, J.C., Calvo, J.P., Rouchy, J.M., 2001. Calcitization of Mg–Ca carbonate and Ca sulphate deposits in a continental Tertiary Basin (Calatayud Basin, NE Spain). Sedimentary Geology 140, 123–142.

Schroll, E., 1996. The Triassic carbonate-hosted Pb–Zn mineralization in the Alps (Europe): the genetic position of Bleiberg type deposit. In: Sangster,

D.F. (Ed.), Carbonate-hosted lead–zinc deposits. SEG Special Publication, vol. 4, pp. 182–194.

Schroll, E., Rantisch, G., 2003. Sulfur isotope pattern in the Bleiberg deposit (Eastern Alps) and its implication for genetically affiliated Pb–Zn deposits. In: Eliopoulos, D.G., et al. (Ed.), Mineral exploration and sustainable development. Millpress, Rotterdam, pp. 1023–1026.

Schuhmacher, M., Fernandes, F., de Chambost, E., 2004. Achieving high reproducibility isotope ratios with the Cameca IMS 1270 in the multi-collection mode. Applied Surface Science 231–232, 878–882.

Seward, T.M., Barnes, H.L., 1997. Metal transport by hydrothermal ore fluids, In: Barnes, H.L. (Ed.), Geochemistry of Hydrothermal Ore Deposits, 3rd edition. Wiley, New York, pp. 435–486.

Sheppard, S.M.F., Charef, A., 1990. Isotopic studies (H, C, O, S, Pb) on carbonate-shale hosted Pb–Zn deposits. In: Pélissonnier, H., Sureau, J.F. (Eds.), Mobilité et concentration des métaux de base dans les couvertures sédimentaires. Manifestations, mécanismes, prospection. Documents du BRGM, vol. 183, pp. 37–49.

Sheppard, S., Charef, A., Boulhel, S., 1996. Diapirs and Pb–Zn mineralization: a general model based on Tunisian (N. Africa) and Gulf Coast (U.S.A.) deposits.

In: Sangster, D. (Ed.), Carbonate-hosted lead–zinc deposits: Society of Economic Geologists, Special Publication Number 4, pp. 230–243.

Southam, G., Saunders, J., 2005. The geomicrobiology of ore deposits. Economic Geology 100, 1067–1084.

Stefanov, St.Hr., Ouchev, A., 1972. Gisement plombo-zincifère de Sidi Driss. Rapport géol. Avec estimation de réserves. Unpublished internal report. Office National des Mines de Tunisie.

Talbi, F., Slim-Shimi, N., Tlig, S., Zargouni, F., 1999. Nature, origine et evolution des fluides dans le district minier de la caldeira d'Oued Bélif (Nefza, Tunisie septentrionale). Comptes-Rendus de l'Académie des Sciences de Paris 328, 153–160.

Vassileff, L., Popov, A., 1979. Formations minérales et zones métallogéniques de la Tunisie. Geologica Acta 7 (4), 43–56.

Zouiten, S., 1999. Application de la géothermométrie chimique aux eaux des sources thermales du Nord de la Tunisie. Unpublished Ph.D. Thesis, Tunis II University, Tunisia, 197 pp.